Invited Speaker

1190 Exploring the dynamics of semiconductors with an ultrafast transmission electron microscope
Sophie Meuret

Oral Presentation

29 Momentum-resolved EELS and CL investigation on 1D-plasmonic crystal fabricated by focused ion beam method
Dr. Akira Yasuhara[1], Masateru Shibata[1], Wakaba Yamamoto[1], Izzah Machfuudzoh[2], Sotatsu Yanagimoto[2], Takumi Sannomiya[2]
[1]JEOL Ltd., Akishima, Japan, [2]Tokyo Institute of Technology, Yokohama, Japan
188 Correlative multi-spectroscopic and microscopic analyses for investigation of UV-C QDs bimodal emission
Dr. Adeline Grenier[1], Dr. Jesus Canaz[2], Mrs Névine Rochat[1], Dr. Zineb Saghi[1], Dr. Jean-Luc Rouvière[3], Dr. Edith Bellet-Almaric[2], Mrs. Audrey Jannaud[1], Dr. Anjali Harikumar[2], Dr. Catherine Bougerol[4], Dr. Lorenzo Rigutti[5], Dr. Eva Monroy[2]
[1]Univ. Grenoble Alpes, CEA, Leti, F-38000 Grenoble, Grenoble, France, [2]Univ. Grenoble-Alpes, CEA, Grenoble INP, IRIG, PHELIQS, 38000 Grenoble, France,, Grenoble, France, [3]Univ. Grenoble Alpes, CEA, IRIG, MEM, 38000 Grenoble, France, grenoble, France, [4]Univ. Grenoble Alpes, CNRS, Grenoble INP, Institut Neel, 38000 Grenoble, France, Grenoble, France, [5]UNIROUEN, CNRS, Groupe de Physique des Matériaux, Normandie Université, 76000 Rouen,France, Grenoble, France
424 Single-crystal and pentatwinned nanorods reverse the handedness of chiral plasmonic nanocrystals: an electron tomography study
Robin Girod[1], Mr. Kyle Van Gordon[2], Dr. Bing Ni[3,4], Dr. Mikhail Mychinko[1], Mr. Francisco Bevilacqua[2], Prof. Luis Liz-Marzan[2,5,6,7], Prof. Sara Bals[1]
[1]EMAT and NANOlab Center of Excellence, University of Antwerp, Antwerp , Belgium, [2]IC biomaGUNE, Basque Research and Technology Alliance (BRTA), Donostia-San Sebastián, Spain, [3]Physical Chemistry, University of Konstanz, Konstanz, Germany, [4]Present address: Department of Chemical Engineering, University of Michigan, Ann Arbor, USA, [5]Centro de Investigación Biomédica en Red, Bioingeniería, Biomateriales y Nanomedicina (CIBER-BBN), Donostia-San Sebastián, Spain, [6]Ikerbasque, Basque Foundation for Science, Bilbao, Spain, [7]CINBIO, University of Vigo, Vigo, Spain
552 New insights into optical property characterization of 2D semiconductor materials through time-correlated photon/electron spectroscopies
Florian Castioni[1], Yves Auad[1], Nadezda Varkentina[1], Alissa Freilinger[1], Steffi Y. Woo[1], Noémie Bonnet[1], Jean-Denis Blazit[1], Xiaoyan Li[1], Marcel Tencé[1], Kenji Watanabe[2], Takashi Taniguchi[3], Odile Stéphan[1], Mathieu Kociak[1], Luiz H. G. Tizei[1]
[1]Université Paris-Saclay, CNRS, Laboratoire de Physique des Solides, Orsay, France, [2]Research Center for Electronic and Optical Materials, National Institute for Materials Science, 1-1 Namiki, , Japan, [3]Research Center for Materials Nanoarchitectonics, National Institute for Materials Science, 1-1 Namiki, , Japan
676 Nanodiamond-based quantum sensing of mechanoregulated metabolic plasticity of cardiac fibroblasts
Dr Aldona Mzyk[1], MSc Ezgi Yilmaz[1], MSc Arthur Dervillez[1], Dr Agostina Crotta Asis[2], Prof. Giovanni D'Angelo[2], Prof. Kirstine Berg-Sørensen[1]
[1]Technical University of Denmark, Kongens Lyngby, Denmark, [2]École Polytechnique Fédérale de Lausanne, , Switzerland
920 Revealing the origin of green light emission in Cs4PbBr6 by cathodoluminescence
Tetsuya Kubota[1], Mr. Sotatsu Yanagimoto[1], Prof. Hikaru Saito[1,2], Dr. Keiichirou Akiba[1,3], Prof. Ayumi Ishii[4], Prof. Takumi Sannomiya[1]

[1]Tokyo Institute of Technology, Yokohama, Japan, [2]Kyushu University, Kasuga, Japan, [3]National Institute for Quantum Science and Technology (QST), Takasaki, Japan, [4]Waseda University, Shinjuku, Japan

Poster Presentation

60 Unlocking Macroscale Solutions with Nanoscale Information:
Towards Next-generation Optoelectronics
Prof Elke Debroye[1], Mr. Handong Jin[1], Mr. Amitrajit Mukherjee[1], Mr. Sudipta Seth[1], Mr. Johan Hofkens[1]
[1]KU Leuven, Department of Chemistry, Leuven, Belgium

89 Second harmonic generation microscopy of femtosecond microstructured crystals
Nuria Sevilla Sierra[1,2], Dr. Javier Rodríguez Vázquez de Aldana[1,2], Dr. Carolina Romero[1,2], Dr. Xavier Mateos[3], Dr. Ignacio Lopez-Quintas[1,2]
[1]Grupo de Investigación en Aplicaciones del Láser y Fotónica, Universidad de Salamanca (USAL), Salamanca, Spain, [2]Unidad de Excelencia en Luz y Materia Estructurada (LUMES), Universidad de Salamanca, Salamanca, Spain, [3]Física i Cristal·lografía de Materials (FiCMA), Universitat Rovira i Virgili (URV), Tarragona, Spain

174 Micro LED performance - a cathodoluminescence study
Mrs Névine Rochat[1], Palmerina González-Izquierdo[1], Davide Zoccarato[1], Fabian Rol[1], Julia Simon[1], Patrick Le Maitre[1], Marion Volpert[1], Matthew Charles[1], Matthieu Lafossas[1], Simona Torrengo[1], Noemie Bonnet[2], Toon Coenen[2], Lukasz Borowik[1]
[1]Univ. Grenoble Alpes, CEA, Leti, Grenoble, France, [2]DELMIC B.V, Delft, The netherlands

384 Electron beam imaging of extremely confined optical modes in topology-optimized dielectric photonic cavities
Dr. Michael Seifner[1,2], M.Sc. Ali Babar[2,3], B.Sc. Anne Sofie Darket[2,3], Assistant Professor Babak Vosoughi Lahijani[2,3], Associate Professor Rasmus Christiansen[2,4], Senior Researcher Elizaveta Semenova[2,3], Professor Søren Stobbe[2,3], Senior Researcher Philip Kristensen[2,3], Senior Researcher Shima Kadkhodazadeh[1,2]
[1]DTU Nanolab, Technical University of Denmark, Kongens Lyngby, Denmark, [2]NanoPhoton - Center for Nanophotonics, Technical University of Denmark, Kongens Lyngby, Denmark, [3]DTU Electro, Technical University of Denmark, Kongens Lyngby, Denmark, [4]DTU Construct, Technical University of Denmark, Kongens Lyngby, Denmark

429 Fabrication of 2-dimensional disordered assemblies of gold nanoparticles and investigation of localized surface plasmon resonances
Kristina Weinel[1,2], Dr. Johannes Schultz[1], Mohammed Fayis Kalady[1], Dr. Daniel Wolf[1], Dr. Leonardo Agudo Jácome[2], Prof. Dr. Axel Lubk[1]
[1]Leibniz-Institut for Solid State and Materials Research Dresden, Dresden, Germany, [2]Federal Institute for Materials Research and Testing, Berlin, Germany

566 Simulating electron energy-loss spectroscopy and cathodoluminescence for nanoparticles located on substrates
Alexander Kichigin[1], Mingjian Wu[1], Stefanie Rechberger[1], Benjamin Apeleo Zubiri[1], Maxim Yurkin[2], Erdmann Spiecker[1]
[1]Institute of Micro- and Nanostructure Research (IMN) & Center for Nanoanalysis and Electron Microscopy (CENEM), Friedrich-Alexander-Universität Erlangen-Nürnberg, IZNF, Erlangen, Germany, [2]CNRS, INSA Rouen Normandie, Univ Rouen Normandie, Normandie Univ, CORIA UMR 6614, Rouen, France

605 Creating free-standing nanostructures with plasmonic properties via Focused Electron Beam Induced Deposition

Di Di Verena Reisecker[1], David Kuhness[1,2], Georg Haberfehlner[1,3], Michele Brugger-Hatzl[3], Robert Winkler[1,2], Anna Weitzer[1], David Loibner[1,2], Martina Dienstleder[3], Gerald Kothleitner[1,3], Harald Plank[1,2,3]
[1]Institute of Electron Microscopy and Nanoanalysis (FELMI), Graz University of Technology, Graz, Austria, [2]Christian Doppler Laboratory DEFINE, FELMI, Graz University of Technology, Graz, Austria, [3]Graz Centre of Electron Microscopy (ZFE), Graz, Austria

837 Control of inter-particle distance between nanoparticles using DNA origami

Jannik Guckel[1,2], Dr Daesung Park[1,2], Dr Markus Etzkorn[2,3], Zhe Liu[2,3], Zunhao Wang[1,2], Dr. Birka Lalkens[2,4]
[1]Physikalisch-Technische Bundesanstalt, Braunschweig, Germany, [2]Laboratory for Emerging Nanometrology (LENA), Braunschweig, Germany, [3]Institute of Applied Physics, Technische Universität Braunschweig, Braunschweig, Germany, [4]Institute of Semiconductor Technology, Technische Universität Braunschweig, Braunschweig, Germany

849 Influence of the deposition parameters on properties of gold plasmonic antennas

Michael Foltýn[1], Marek Patočka[1], Rostislav Řepa[1], Tomáš Šikola[1], Michal Horák[1]
[1]Brno University of Technology, Brno, Czech Republic

915 Analysis of photon bunching in coherent cathodoluminescence

Mr Sotatsu Yanagimoto[1], Dr Naoki Yamamoto[1], Dr Takumi Sannomiya[1], Dr Keiichirou Akiba[1,2]
[1]Tokyo Institute of Technology, Nagatsuta, Midoriku, Yokohama,, Japan, [2]National Institutes for Quantum Science and Technology, Watanuki, Takasaki, Japan

945 Resonant inelastic light scattering micro-spectroscopy to probe inter-moiré miniband excitations in twisted 2D semiconductors

Dr. Nihit Saigal[1,2], Dr. Lennart Klebl[3], Mr. Hendrik Lambers[1], Mr. Sina Bahmanyar[1], Mr. Veljko Antić[1], Prof. Dante Kennes[4,5], Prof. Tim Wehling[3,6], Prof. Ursula Wurstbauer[1,7]
[1]Institute of Physics, University of Münster, Wilhelm-Klemm-Str. 10, 48149 Münster, Germany, Münster, Germany, [2]EMBL Imaging Center, European Molecular Biology Laboratory, Meyerhofstr. 1, 69117 Heidelberg, Germany, Heidelberg, Germany, [3]Institute of Theoretical Physics, University of Hamburg, Notkestrasse 9, 22607 Hamburg, Germany, Hamburg, Germany, [4]Institute for Theory of Statistical Physics, RWTH Aachen University, and JARA Fundamentals of Future Information Technology, 52062 Aachen, Germany, Aachen, Germany, [5]Max Planck Institute for the Structure and Dynamics of Matter, Center for Free Electron Laser Science, 22761 Hamburg, Germany, Hamburg, Germany, [6]The Hamburg Centre for Ultrafast Imaging, 22761 Hamburg, Germany, Hamburg, Germany, [7]Center for Soft Nanoscience (SoN), Busso-Peus-Str. 10, 48149 Münster, Germany, Münster, Germany

953 Study of nanolaser optical and structural properties at the nanometer scale

PhD Student Cléo Santini[1], Nika van Nielen[2], Pierre-Marie Coulon[3], Stéphane Vézian[3], Julien Brault[3], Philip A. Shields[5], Albert Polman[2], Benjamin Damilano[3], Christelle Brimont[4], Thierry Guillet[4], Sophie Meuret[1]
[1]CEMES, Toulouse, France, [2]AMOLF, Amsterdam, Netherlands, [3]CRHEA, Valbonne, France, [4]L2C, Montpellier, France, [5]University of Bath, , United Kingdom

957 Improved conventional TEM sample preparation exploiting the birefringence of materials

Aleksander Brozyniak[1], Karin Stadlmann[1], Philipp Kürnsteiner[1], Heiko Groiss[1]
[1]Christian Doppler Laboratory for Nanoscale Phase Transformations, Center for Surface and Nanoanalytics, Johannes Kepler University Linz, Linz, Austria

1003 Investigating the photoelectronic properties of MoS2 thin layer with ITO nanoparticles using photoluminescence and cathodoluminescence

Mr Andrea Cicconardi[1,2], Dr Andrea Griesi[1], Dr Gunnar Kusch[4], Dr Silvia Dante[1], Prof Rachel Oliver[4], Dr Ilka Kriegel[1,3], Dr Giorgio Divitini[1]
[1]Istituto Italiano di Tecnologia, Genova, Italy, [2]University of Genova, Genova, Italy, [3]Istituto Italiano di Tecnologia, Turino, Italy, [4]University of Cambridge, Cambridge, United Kingdom

1024 Structural and Compositional Investigation of Ag-Incorporated CsPbBr3 Nanocrystal Heterostructures
Dr Sirous Khabbaz Abkenar[1], Ms. Anna Cabona[2,3], Mr. Basem Ameen Ahmed Qahtan[1,3], Dr. Stefano Toso[2], Dr. Andrea Griesi[1], Prof. Liberato Manna[2], Dr. Giorgio Divitini[1]
[1] Istituto Italiano di Tecnologia, Electron Spectroscopy and Nanoscopy, Genova, Italy, [2]Istituto Italiano di Tecnologia, Nanochemistry, Genova, Italy, [3]Dipartimento di Chimica e Chimica Industriale, Università degli Studi di Genova, Genova, Italy
1091 Microstructure of light-emitting phosphor of (Sr, Ca)AlSiN3:Eu2+
Hajime Matsumoto[1]
[1]Mitsubishi Chemical Corp., Yokohama, Japan, [2]National Institute for Materials Science, Tsukuba, Japan
1093 Multifunctional hybrid nanocomposite films: linking inorganic nanoparticles using α-synuclein as molecular linker
Prof Patrizia Canton[1], Prof Adolfo Speghini[2], Dr Emil Milan[2], Dr R Tira[2], Dr. M. D'Onofrio[2], Dr M Assfalg[2]
[1]Department of Molecular Sciences and Nanosystems, Ca' Foscari University of Venice , Venezia, Italy, [2]Department of Biotechnology, University of Verona, Verona, Italy

Late Poster Presentation

1221 Visualization of surface plasmon propagation and emissions by cathodoluminescence
Izzah Machfuudzoh[1], Sotatsu Yanagimoto[1], Researcher Naoki Yamamoto[1], Supervisor Takumi Sannomiya[1]
[1]Tokyo Institute of Technology, Yokohama, Japan
1316 Fabrication and charaterization of plasmonic nanopillars on a thin membrane for TEM investigation
Maria Serra González[1], Matthias Keil[1], Rucha Deshpande[1], Rafael Taboryski[1], Shima Kadkhodazadeh[1]
[1]DTU Nanolab, Kongens Lyngby, Denmark
1215 HR STEM study of anion/cation exchange in colloidal lead halide perovskite heterostructures
Iurii Ivanov[1], Mr Nikolaos Livakas[2], Ms Juliette Zito[2], Dr. Ivan Infante[3], Prof. Liberato Manna[2], Dr. Giorgio Divitini[1]
[1]Electron Spectroscopy and Nanoscopy, Istituto Italiano di Tecnologia, , , [2]Nanochemistry, Istituto Italiano di Tecnologia, , , [3]BCMaterials, Basque Center for Materials, Applications, and Nanostructures, Ikerbasque, Basque Foundation for Science, ,

1190

Exploring the dynamics of semiconductors with an ultrafast transmission electron microscope

Sophie Meuret

PS-11, Lecture Theater 2, august 28, 2024, 14:00 - 16:00

29

Momentum-resolved EELS and CL investigation on 1D-plasmonic crystal fabricated by focused ion beam method

Dr. Akira Yasuhara[1], Masateru Shibata[1], Wakaba Yamamoto[1], Izzah Machfuudzoh[2], Sotatsu Yanagimoto[2], Takumi Sannomiya[2]
[1]JEOL Ltd., Akishima, Japan, [2]Tokyo Institute of Technology, Yokohama, Japan

PS-11, Lecture Theater 2, august 28, 2024, 14:00 - 16:00

Background and aims;
Plasmonic crystals with periodic structures constructed from plasmonic materials have been widely investigated, as they exhibit attractive optical properties based on surface plasmon polaritons (SPPs). To explore the optical properties of plasmonic crystals at the nanoscales, electron energy loss spectroscopy (EELS) and cathodoluminescence (CL) techniques based on scanning transmission electron microscopy (STEM) are the two complimentary approaches; EELS gives the information on the excitation process and thus allows accessing the optical information outside the light line while CL gives information of the photon emission meaning the information inside the light line. With the angle-dependent detection, momentum-resolved spectra, i.e. dispersion relations, can be obtained by both techniques. In this study, we fabricated a one-dimensional plasmonic crystal (1D-PIC) from Al using a focused ion beam (FIB) method and thoroughly investigate their optical properties using momentum-resolved EELS and CL methods.
Methods;
1D-PIC was fabricated using a JIB-PS500i instrument (FIB-SEM system) with a focused Ga-ion beam. At first, an Al thin lamella consisting of large grains(> um) was prepared out of bulk Al to ensure the sufficient propagation of SPPs. The periodic structure was then carved with a precise control of the ion beam dose to create the terrace and trench structures using the specimen drift compensation function to prevent structural sagging. To analyze the optical properties, a JEM-ARM200F(TEM/STEM) instrument with GIF Continuum ER was used for the momentum-resolved EELS, and a modified JEM-2100F(TEM/STEM) instrument with a dedicated CL measurement system was used for the momentum-resolved CL.
Results;
Figure 1a shows TEM BF image of Al 1D-PIC, confirming the successful fabrication of the periodic structure of 500 nm periodicity with the terraces and trenches of the same width. Panels b and c in Fig.1 show the momentum-resolved EELS and CL spectra of Al 1D-PIC, where the dispersion relations of SPs are clearly visualized. The superimposed curves in panels b and c display the calculated dispersion of Al SPPs. The light lines are also indicated on images by yellow dotted lines. It is noted that EELS has the capability of accessing the information outside of light line, while the CL technique can investigate only the photon information inside of the light line. On the other hand, the CL technique has a strong advantage to achieve both nanoscopic spatial resolution and momentum resolution by utilizing the electron beam for the spatial resolution and photon detection for the momentum detection. The employed CL equipment allows acquiring the momentum-resolved CL spectrum at each electron beam position while scanning the electron beam, thus producing four-dimensional (4D) CL data set. In the EELS result, shown in Fig. 1b, enhanced horizontal lines along the momentum axis with 2.6, 5.0, and 6.5 eV are visible, which can be assigned as the localized surface plasmon modes. These local modes can be understood from the resonance conditions where the SPPs make standing waves with different orders matching the local structure of 1D PIC. The momentum-resolved CL results, as shown in Fig. 1 c, display the dispersion relation reproduced from the upward photon emission from the specimen. Since the periodic structure is constructed on the top surface of the specimen, dispersion lines are clearly visible only in the upward emission. In

addition to the dispersion line depicted in Figure c, discernible local mode around 2.6 eV, extending the intensity in the momentum direction, is also evident.

Conclusion;

We have successfully fabricated the 1D-PIC using the FIB technique out of large grains of Al. The presence of SPP and local modes on the 1D-PIC were confirmed using the EELS and CL techniques. Furthermore, through the momentum-resolved EELS and CL mapping analysis, we identified the dispersion relations of SPPs and local modes. Through the combination of momentum-resolved EELS and CL measurements, comprehensive investigations can be performed, which allows accessing the optical properties of nanostructures far beyond the diffraction limit of light.

Figure caption;

Figure.1 (a) TEM BF image of the Al 1D-PIC fabricated by the FIB method. A schematic illustration of the structure is shown in the inset. (b) Momentum-resolved EELS result. The dashed circles indicate the diffraction spot positions reflecting the period of the 1D PIC. The backgrounds of EELS signals are subtracted from the original data. (c) Momentum-resolved CL spectrum acquired in the upward direction (structured side). The CL spectrum is obtained by spatially integrating the CL signal over the 1D plasmonic crystal.

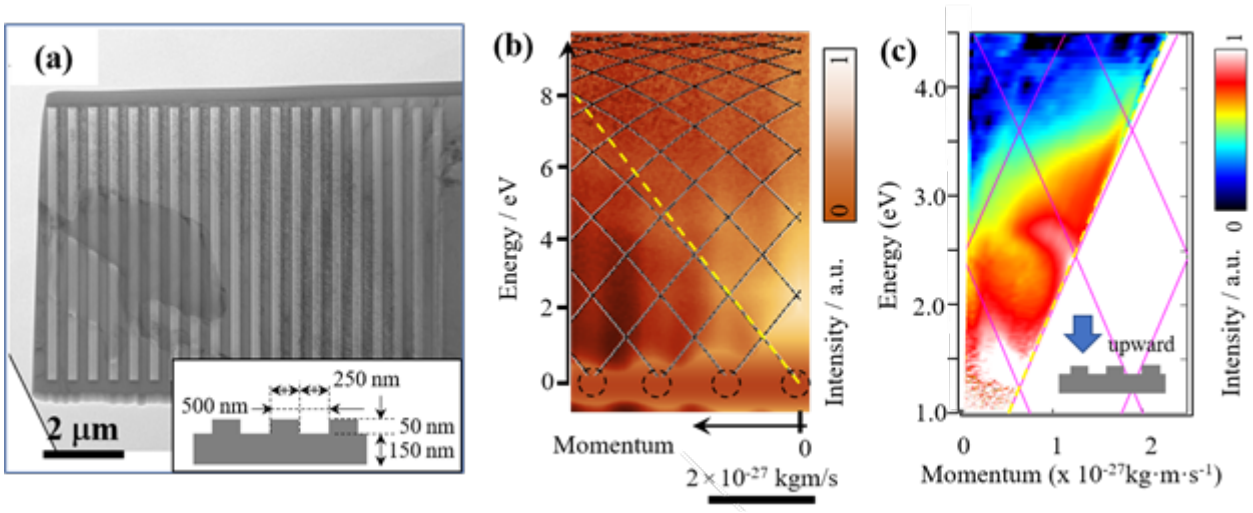

Keywords:

mometum-resolved, EELS, cathodoluminescence, CL, plasmon

188

Correlative multi-spectroscopic and microscopic analyses for investigation of UV-C QDs bimodal emission

Dr. Adeline Grenier[1], Dr. Jesus Canaz[2], Mrs Névine Rochat[1], Dr. Zineb Saghi[1], Dr. Jean-Luc Rouvière[3], Dr. Edith Bellet-Almaric[2], Mrs. Audrey Jannaud[1], Dr. Anjali Harikumar[2], Dr. Catherine Bougerol[4], Dr. Lorenzo Rigutti[5], Dr. Eva Monroy[2]
[1]Univ. Grenoble Alpes, CEA, Leti, F-38000 Grenoble, Grenoble, France, [2]Univ. Grenoble-Alpes, CEA, Grenoble INP, IRIG, PHELIQS, 38000 Grenoble, France,, Grenoble, France, [3]Univ. Grenoble Alpes, CEA, IRIG, MEM, 38000 Grenoble, France, grenoble, France, [4]Univ. Grenoble Alpes, CNRS, Grenoble INP, Institut Neel, 38000 Grenoble, France, Grenoble, France, [5]UNIROUEN, CNRS, Groupe de Physique des Matériaux, Normandie Université, 76000 Rouen,France, Grenoble, France

PS-11, Lecture Theater 2, august 28, 2024, 14:00 - 16:00

Background and aims
There is a strong interest in the development of efficient solid-state UV-C sources in the 220-270 nm range due to their powerful germicidal properties. Light emitting diodes (LEDs) based on the AlGaN semiconductor system are the most promising approach, but the early stage of development of the AlGaN technology still presents challenges, such as inefficient p-type doping and resistive ohmic contacts, resulting in low efficiencies. An approach that circumvents these material limitations is the use of electron beam pumped lamps; with a UV-emitting material (anode) housed in a vacuum tube. High-energy electrons are emitted from a cold cathode and accelerated towards the semiconductor anode, generating free carriers. Unlike LEDs, electron beam pumped lamps don't require p-type doping or contacts. To further enhance device performance, the use of AlGaN quantum dots (QDs) as radiative recombination centers is very promising. The three-dimensional (3D) carrier confinement within QDs prevents carrier diffusion towards non-radiative centers, leading to improved radiative efficiency even at high temperatures. However, samples emitting at wavelengths shorter than 270 nm present broad or bimodal spectra. It is crucial to minimize bimodal emission or emission line width to achieve highly efficient devices for disinfection.
In this work, we investigate the origin of the bimodal emission in Al0,14Ga0,86N/AlN QD superlattices designed for electron beam pumped UV emitters. We propose a comprehensive analysis combining 2D-3D scanning transmission electron microscopy (STEM), atom probe tomography (APT), cathodoluminescence (CL) spectroscopy associated to 3D simulations of the electronic structure.
Methods
The sample consists of 100 periods of Al0,14Ga0,86N/AlN self-assembled Stranski-Krastanov QDs deposited on commercial 1-µm-thick (0001)-oriented AlN-on-sapphire templates by plasma assisted molecular beam epitaxy (MBE) [Fig.1(b)]. 2D and 3D structural properties of the samples were studied by bright field (BF) and high-angle annular dark field (HAADF) STEM imaging using a probe-corrected Titan Themis (Thermo Fisher Scientific) operating at 200 kV. Compositional information of the sample was measured by laser-assisted atom probe tomography using a CAMECA FlexTAP instrument. Cathodoluminescence measurements were carried out using an Attolight CL-dedicated SEM microscope. The electronic structure of the QDs was modelled using the Nextnano3 8-band k·p Schrödinger-Poisson equation solver with AlN and GaN parameters and experimental dimensions and composition as inputs parameters.
Results
The top-view CL [fig.2(a)] presents a predominant line at 290 nm and a secondary emission at 305 nm. The SEM (scanning electron microscopy) image associated to the λ-filtered CL map [Fig.2(b)] evidences that the emission at longer wavelengths is linked to pits.

To gain deeper understanding of the structural and optical effects associated with the pits observed at the surface, we performed CL and transmission electron microscopy (TEM) characterization on the same TEM sample. Figure 3(a) presents a λ-filtered CL map of a zoomed region with two wavelength emission domains superimposed to a HAADF-STEM image of the same region. The associated HAADF-STEM image [Fig. 3(b)] shows that the longer wavelength emission appears associated with 3D conical structures.The zoomed BF-STEM image ([fig.3(c)] of a conical structure shows that it appears at the interface between the AlN buffer layer and the superlattice with inclined facets around 30° with the (0001) plane at the edge. To gain further insight into the nature and compostion of the conical domains, electron tomography has been performed and shows the propagation of the shallow pit profile through the superlattice [Fig.4(a)], with a brighter chemical-related contrast indicating a higher Ga content compared to the surrounding regions. In addition, HAADF-HRTSEM has allowed to determine the dimension of QDs in conical and homogeneous (non conical) emission regions.

APT was performed to gain combined 3D structural and quantitative compositional information within the conical structure. Figure 4(b) displays an APT Ga map; which enables the visualization of the QD planes, as they are those containing Ga. The upper part of the tip exhibits a homogeneous region with flat QD planes. However, a significant portion of the tip contains a threading defect which corresponds to the faceted step present at the boundary of the cone-shaped extended defect. Focusing on the APT analysis of 5 QD planes [Fig. 4(c)] located on the lower part of the sample, the Ga-atom planes exhibit a bending angle of approximately 30°, corresponding to the behavior observed in bright field (BF) STEM [Fig.4(d)]. Projected side and top view Ga map density for the 5 QD layers are presented in the figure 4(e) and (f), respectively. We see that the QD layers exhibit a Ga enrichment towards the 30° facet. We choose to quantify the composition of the QD-SL in the defect and homogenous region by the comparison of the Ga density. Considering that the non-defective regions contain Al0.14Ga0.86N QDs (nominal concentration deduced from growth conditions), we deduce that the faceted region should contain Al0.07Ga0.93N QDs, which should red shift the emission wavelength.

To investigate whether the chemical and morphological changes of the QD population within the entire structure are responsible for the emission bimodality, we conducted 3D simulations of the electronic structure of AlGaN/AlN QDs by solving the Poisson and Schrödinger equations using Nextnano3 within the conical and homogeneous regions. Dimensions and composition in (i) homogeneous [Fig.5 (a)], (ii) conical area [Fig.5 (b)] and (iii) at the frontier of the defect area with 30°-facet [Fig.5 (c)] are used as inputs parameters for simulations. The direct comparison between simulated and experimental wavelength in both regions [Fig. 5(d)] confirms that the bimodality emission is due to the different size and chemistry of the dots within the defect and at the defect boundary.

Conclusion

The bimodal emission is attributed to the presence of a secondary population of quantum dots located within cone-like structural defects. These defects emerge at the initial interface between the AlN buffer layer and the QD superlattice and propagate vertically. They are associated to a dislocation featuring a strong strain field, thereby facilitating the generation of a shallow pit characterized by 30° faceted boundaries.

Fig. 1: Electron pumped UV-C light emitter

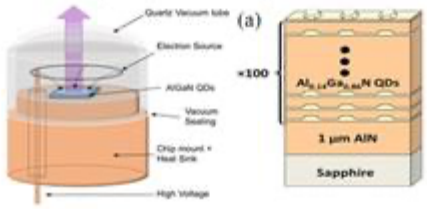

Fig. 2: Optical signature of the UV-C light emitter

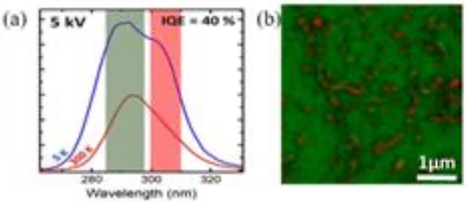

⟹ Bimodal emission

Fig. 3: Structural combined with optical signature

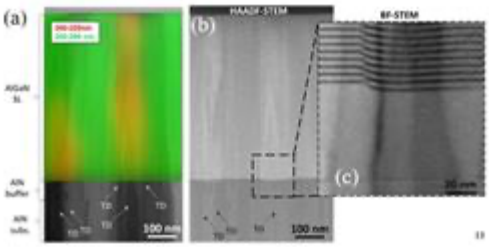

⟹ Conical structure responsible for the 2nde emission.

Fig. 4: Morphological and chemical analysis of the conical structure

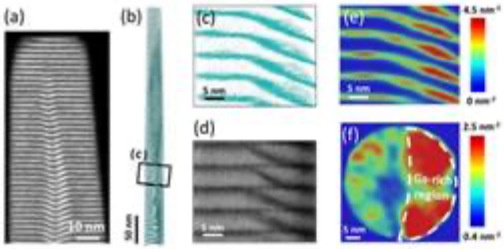

⟹ Morphology and Ga density within the conical structure.

Fig. 5: Band structure simulations using experimental features

(a) Homogeneous area (b) Conical area (c) $Al_XGa_{1-X}N$/AlN QDs SL

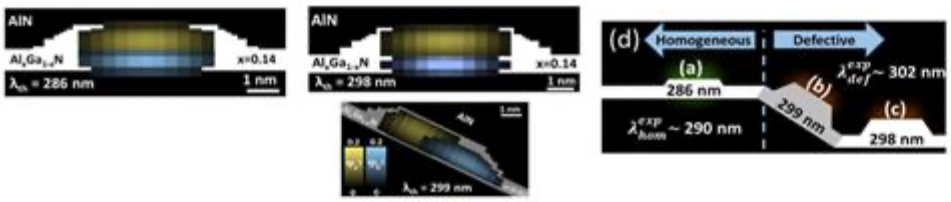

⟹ Confirmation of the impact of dimension and composition variation of the QD's population on the bimodal emission.

Keywords:

UV-QDs, bimodal emission, correlative microscopy

Reference:

[1]: J. Canaz et al., under review, ACS NANO.
[2]: This work, performed on the Platform for Nanocharacterisation (PFNC), was supported by the "Recherche Technologique de Base" and "France 2030 - ANR-22-PEEL-0014" programs of the French National Research Agency (ANR).
[3]: This project received funding from the French National Research Agency via the ASCESE-3D and FUSSL projects (ANR-21-CE50-0016 and ANR-22-CE09-0024).

424

Single-crystal and pentatwinned nanorods reverse the handedness of chiral plasmonic nanocrystals: an electron tomography study

Robin Girod[1], Mr. Kyle Van Gordon[2], Dr. Bing Ni[3,4], Dr. Mikhail Mychinko[1], Mr. Francisco Bevilacqua[2], Prof. Luis Liz-Marzan[2,5,6,7], Prof. Sara Bals[1]
[1]EMAT and NANOlab Center of Excellence, University of Antwerp, Antwerp , Belgium, [2]IC biomaGUNE, Basque Research and Technology Alliance (BRTA), Donostia-San Sebastián, Spain, [3]Physical Chemistry, University of Konstanz, Konstanz, Germany, [4]Present address: Department of Chemical Engineering, University of Michigan, Ann Arbor, USA, [5]Centro de Investigación Biomédica en Red, Bioingeniería, Biomateriales y Nanomedicina (CIBER-BBN), Donostia-San Sebastián, Spain, [6]Ikerbasque, Basque Foundation for Science, Bilbao, Spain, [7]CINBIO, University of Vigo, Vigo, Spain

PS-11, Lecture Theater 2, august 28, 2024, 14:00 - 16:00

Background and aims.
Nanomaterials with chiroptical properties absorb differently left- and right-handed light, an asymmetry that is reinforced by the local surface plasmon resonance of metallic nanoparticles. The synthesis of such chiral particles with controlled shapes and optical properties is of major interest for a host of potential applications including bio-sensing, therapeutics or catalysis, and can be realized by transferring chirality from an organic inducer to the inorganic material in seed-mediated colloidal synthesis [1,2]. Usually, the handedness of the inducer is thought to be transferred to the product [1]. However, recent studies showed that the geometry of the achiral seeds can also influence handedness, even if the same inducer is used [3], and it remains unclear if such effect is related to morphological or structural (surface facets, twin boundaries, defects, …) properties.
Here, we aimed to understand the effect of the seeds on the growth of chiral features. Specifically, we investigated the growth starting on well-defined single-crystal (SC) or penta-twinned (PT) gold nanorod (NR) seeds. To uncover the complex morphological changes at the nanoscale, we used electron tomography (ET), a method that enables three-dimensional (3D) reconstructions down to the atomic scale. In two different synthesis protocols, micelle-templated or chemically induced, 3D reconstructions and nanoscale morphological analysis showed that the final products had reverse handedness and strong morphological differences when using PT or SC seeds [4].
Methods.
We studied the growth of chiral features on well-controlled achiral gold seeds synthesized by wet chemistry. The two systems investigated here were PT NRs featuring five {100} lateral facets and caped by {111} facets at the tips, and SC NRs with an octagonal cross-section, {520} lateral facets and {110} and {100} tips. Chiral features were grown by two protocols. The chemically induced pathway used the chiral L-cystine (L-cys) amino-acid, which was previously reported to yield highly twisted structures on SC seeds [2]. The micelle-templated protocol used chiral, worm-like micelles formed by (S)-1,1'-binaphthyl-2,2-diamine (S-BINAMINE) and cetyltrimethylammonium chloride (CTAC), that are known to yield wrinkled, helical, NRs [1]. The optical properties of the seeds and of the products were characterized by extinction spectroscopy and circular dichroism (CD) measurements.
To characterize the morphology and structure of the final products, we used ET, whereby projection images acquired at incremental tilt-angles are used to compute a 3D reconstruction of the object. Tilt-series were acquired in 2-3° increments and in scanning transmission electron microscopy (STEM) high angle annular dark field (HAADF) mode to provide mass-thickness contrast and meet the requirements for accurate reconstructions. The reconstructions were computed using an expected maximization (EM) algorithm or a constraint SIRT approach developed in-house and implemented in Matlab with the ASTRA toolbox. Morphological analyses included helicity measurements and orientation tracking. Helicity uses a surface mesh extracted from reconstructions to compute a pseudoscalar metric indicating how close to a perfect helix the shape is and its handedness (positive

helicity means right-handed, negative means left-handed) [5]. Orientation tracking reveals the dominant orientation of features around a NR to study the local variations of chirality and was implemented using a combination of the ImageJ OrientationJ plugin and in-house code.

Results.

Regardless of the synthetic pathway, starting from PT or SC seeds resulted in products with opposite signs in CD spectra, indicating a reverse handedness. Strong discrepancies were further seen in the morphology of the particles, as reconstructed in ET. With the L-Cys protocol, SC seeds resulted in strongly twisted NRs with clear right-handed morphology (Figure, a). This observation was supported by helicity measurements, showing strongly positive values. On the other hand, PT seeds resulted in poorly defined, highly complex shapes with no obvious handedness (Figure, b). Helicity measurements were typically weak, with a complex combination of right and left-handed features in each particle leading to some NRs exhibiting a dominantly left handedness and others with right handedness (Figure, b). This observation suggests that optical handedness is not limited to helical features. Overall, a strong influence from the seed crystal structure was expected in this growth protocol, as chirality emerges through the preferential growth of chiral facets stabilized by the chiral inducer. More surprisingly, micelle-templated NRs grown from PT seeds also had an opposite sign in CD spectra as compared to their SC counterpart. ET reconstructions showed closely resembling wrinkled morphologies in both cases, with a major difference in the orientation of the wrinkles (Figure, c, d). PT NRs showed left-handed wrinkles, coherently with positive g-factor plots, while SC NRs showed right-handed features. Helicity measurements confirmed this observation by showing close absolute values but opposite signs.

To further probe how the morphology of the seeds was impacting the final micelle-templated products, we assessed if the presence of corners and lateral facets influenced the wrinkle morphology beyond the global particle handedness. Notably, the tips featured better aligned wrinkles on SC NRs, and wrinkles on the lateral facets grew at different angles. Tracking the dominant orientation of wrinkles around the particles also revealed that PT NRs retained a 5-fold symmetry with alternating areas of flat and oriented wrinkles (Figure, c, d). In contrast, SC NRs had a 4-fold symmetry with similarly alternating flat and oriented wrinkles, coherent with an intermediate with square cross-section we previously identified. These observations confirm that the way micelles adsorb on the seeds' surface is influenced by geometrical (angles, number of facets) or crystallographic (facet index) consideration, in turn impacting the orientation of wrinkle growth and, likely, the handedness of the particle.

Conclusion.

We used ET and detailed nanoscale morphological analyses to show that the nature of the achiral seed in chiral seeded growth has a major influence on the handedness of the products and on their chiroptical properties. Furthermore, this observation in micelle-templated growth shows that wrinkle growth is not random but influenced by geometrical or crystallographic factors. This work enhances the toolbox for controlling chirality at the nanoscale and demonstrates the benefits of ET in linking morphology and optical properties, supporting the development of novel optical nanomaterials.

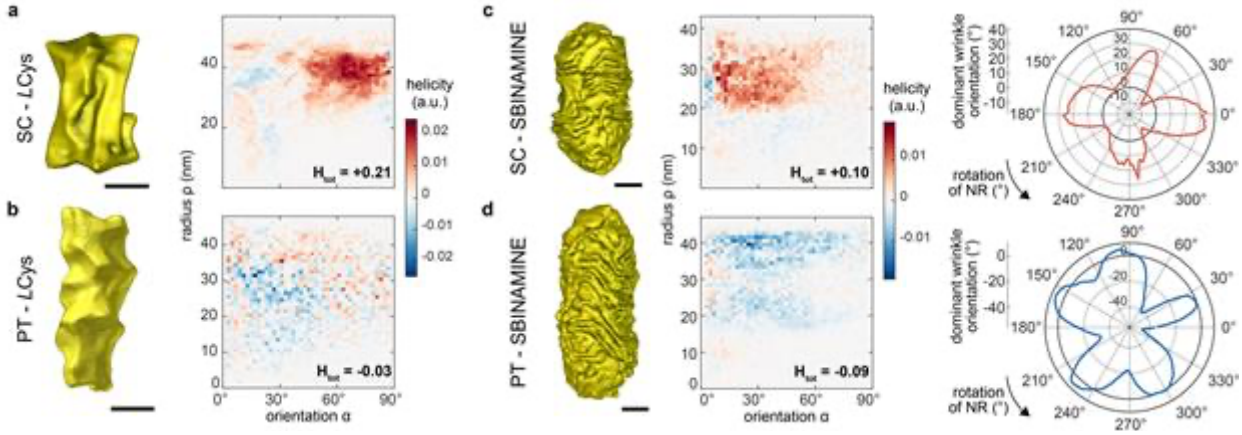

Keywords:

TEM, tomography, chirality, plasmonics, nanorods

Reference:

1. González-Rubio, G. et al. Micelle-directed chiral seeded growth on anisotropic gold nanocrystals. Science 368, 1472–1477 (2020).
2. Ni, B. et al. Chiral Seeded Growth of Gold Nanorods Into Fourfold Twisted Nanoparticles with Plasmonic Optical Activity. Advanced Materials 35, 2208299 (2023).
3. Sun, X. et al. Tunable Reversal of Circular Dichroism in the Seed-Mediated Growth of Bichiral Plasmonic Nanoparticles. ACS Nano 16, 19174–19186 (2022).
4. Van Gordon, K. et al. Single Crystal and Pentatwinned Gold Nanorods Result in Chiral Nanocrystals with Reverse Handedness. Submitted.
5. Heyvaert, W. et al. Quantification of the Helical Morphology of Chiral Gold Nanorods. ACS Materials Lett. 4, 642–649 (2022).

552

New insights into optical property characterization of 2D semiconductor materials through time-correlated photon/electron spectroscopies

Florian Castioni[1], Yves Auad[1], Nadezda Varkentina[1], Alissa Freilinger[1], Steffi Y. Woo[1], Noémie Bonnet[1], Jean-Denis Blazit[1], Xiaoyan Li[1], Marcel Tencé[1], Kenji Watanabe[2], Takashi Taniguchi[3], Odile Stéphan[1], Mathieu Kociak[1], Luiz H. G. Tizei[1]
[1]Université Paris-Saclay, CNRS, Laboratoire de Physique des Solides, Orsay, France, [2]Research Center for Electronic and Optical Materials, National Institute for Materials Science, 1-1 Namiki, , Japan, [3]Research Center for Materials Nanoarchitectonics, National Institute for Materials Science, 1-1 Namiki, , Japan

PS-11, Lecture Theater 2, august 28, 2024, 14:00 - 16:00

Background: The optical properties of luminescent materials are intricately tied to their structural and chemical characteristics at the nanometric, or even atomic scale. Understanding this relationship has long relied on the combination of scanning transmission electron microscopy (STEM) with external optical techniques such as absorption or photoluminescence spectroscopies, probing the excitation and emission mechanisms at the micrometric scale. However, the significant gap in spatial resolution between these methods and phenomena of interest often leads to ambiguous or even impossible interpretations of the measurements. Recent advancements in nano-optics seek to address this resolution disparity by enabling observation of luminescent material properties at nanometric scales. In that sense, STEM has undergone substantial instrumental and theoretical progress, providing valuable insights into optical properties through conventional inelastic electron scattering (electron energy loss spectroscopy, EELS) and photon emission (cathodoluminescence, CL) spectroscopies [1]. However, both techniques are hindered by spectral resolution limitations and the broadband excitation process of the electron beam. This contribution investigates the possibilities presented by the latest advancements in STEM techniques, specifically focusing on electron-photon time-correlations.
Methods: To overcome these challenges, two techniques currently in development will be highlighted in this contribution:

- Cathodoluminescence Excitation Spectroscopy (CLE, Figure 1b), based on coincidence measurements between EELS and CL events. CLE offers insights into energy transfer pathways and excitation lifetimes at the nanometer scale, as previously reported [2,3].
- Electron Energy Gain Spectroscopy (EEGS, Figure 1c), an extension of the photon-induced near-field electron microscopy (PINEM) technique, investigates primary electron acceleration when the beam interacts with a strong optical field generated by a laser. By changing the energy of the photons, this technique can resolve ultra-fine optical resonances in the sub-meV range, revealing novel physical properties below the energy resolution achievable with state-of-the-art monochromated electron beams. So far, it has only been applied to photonic excitations, such as plasmons or surface polaritons [4].

Results and Conclusion: These techniques, with their distinct excitation and deexcitation processes (Figure 1a), are expected to be highly complementary, offering deeper insights into optical mechanisms at the nanometer scale. The present contribution focuses on using transition metal dichalcogenides (TMDs) as a model system of functional luminescent material to explore the insights provided by these correlated techniques.

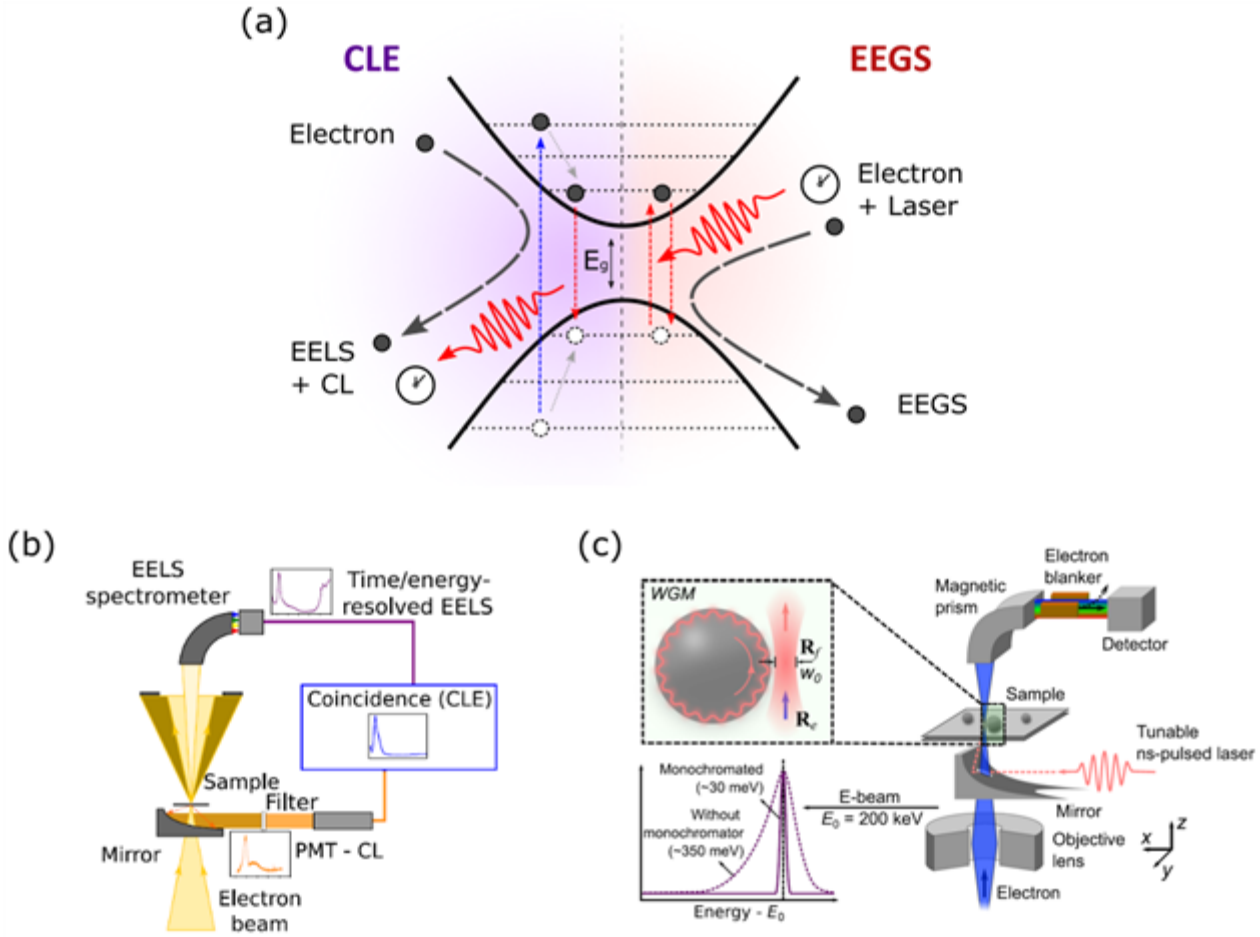

Keywords:

Nano-optic, electron/photon spectroscopy, semiconductor TMD.

Reference:

[1] N. Bonnet et al., Nano Lett. 21 (2021) 10178–10185.
[2] N. Varkentina et al., Sci. Adv. 8 (2022) eabq4947.
[3] N. Varkentina et al., Appl. Phys. Lett. 123 (2023) 223502.
[4] J.-W. Henke et al., Nature 600 (2021) 653–658.
[5] Y. Auad, Nat Commun 14 (2023) 4442.

676

Nanodiamond-based quantum sensing of mechanoregulated metabolic plasticity of cardiac fibroblasts

Dr Aldona Mzyk[1], MSc Ezgi Yilmaz[1], MSc Arthur Dervillez[1], Dr Agostina Crotta Asis[2], Prof. Giovanni D'Angelo[2], Prof. Kirstine Berg-Sørensen[1]
[1]Technical University of Denmark, Kongens Lyngby, Denmark, [2]École Polytechnique Fédérale de Lausanne, , Switzerland

PS-11, Lecture Theater 2, august 28, 2024, 14:00 - 16:00

Background incl. aims

Quantum sensing is one of the most advanced quantum technologies. Quantum sensors based on single electronic spins, or small spin ensembles, can deliver nanoscale spatial resolution in detecting magnetic fields. This property has been exploited in breakthrough experiments in the biomedical field ranging from localised detection of free radicals [1] or temperature [2] inside living cells, the demonstration of magnetic resonance imaging on picoliter samples [3], to the identification of HIV with >10^5 better sensitivity than classical methods [4]. However, we have only just started scratching the surface of the application potential of quantum technology into biomedical research and development. Our group has been developing novel nanodiamond-based quantum sensing protocols to investigate mechanoregulation of metabolism at sub-cellular level. In this study, we have focused on the mechanoregulation in the heart scar formation. The myocardial scar formation known as cardiac fibrosis is a key contributor to heart failure. Anti-fibrotic therapies are still under development due to limited understanding of molecular processes behind scar formation. The cardiac fibrosis starts with changes in the mechanical properties of a heart extracellular matrix (ECM), which leads to transdifferentiation of cardiac fibroblasts (quiescent stage) into myofibroblasts (activated stage). We have very little knowledge about how mechanical stimuli govern fibroblasts metabolic plasticity. Free radicals (FRs), a class of reactive molecules with an unpaired electron, have emerged to be crucial for intracellular signalling. However, as FRs are short lived and difficult to detect with the state-of-the art-methods, therefore their role in cardiac metabolic plasticity remained unknown. In our studies, we aimed to reveal the role of FRs in lipid plasticity of cardiac fibroblasts in response to mechanical stimuli with quantum sensors.

Methods

The experiments were performed on primary human cardiac fibroblasts cultured on stiff (Young modulus >10 kPa) and soft (Young modulus <10 kPa) substrates to stimulate their activation. All experiments were performed for young (2nd passage) and aged cells (>5th passage). We used a quantum sensing technique called T1 relaxometry [5] to detect changes in free radical generation by mitochondrial networks. Fluorescent nanodiamonds (FNDs) with NV- centers were used as sensors. We modified the surface of the nanodiamonds with antibody for targeting their delivery to mitochondria. Then we checked the uptake efficiency and colocalization of FNDs with mitochondria and transporting vesicles inside the cells. In these studies, the T1 relaxometry was for the first time combined with optical trapping of FNDs to simultaneously measure FRs and viscoelastic properties of mitochondrial networks. We further evaluated changes in lipidome with single cell lipidomics using MALDI mass spectrometry imaging and fluorescent imaging of stained lipids.

Results

Our studies have demonstrated that uptake of the nanodiamond sensors depends on the age of cells and stiffness of the substrate. We have shown successful targeting of FNDs to mitochondria, which was independent of age of cells and substrate stiffness. We have found that FR generation by mitochondrial networks shows some dependence on the age of the cells and also indicate mechanoregulation. Furthermore, the mechanical stimulation and age of cardiac fibroblasts influence heterogeneity of lipotypes and their distribution across the population of quiescent and activated cells. We have shown lipotype correlation with the FRs level and viscoelastic properties of mitochondrial networks.

Conclusion

As a result, our research shed light on the mechanobiology of the heart scarring process. We have proven that quantum sensing combined with optical trapping can be used to study mechanoregulation of metabolic plasticity of cardiac fibroblasts. Our simple quantum sensing model of mechanoregulated cardiac fibrosis could be further developed towards 3D cell cultures and serve as screening platform for metabolic drugs.

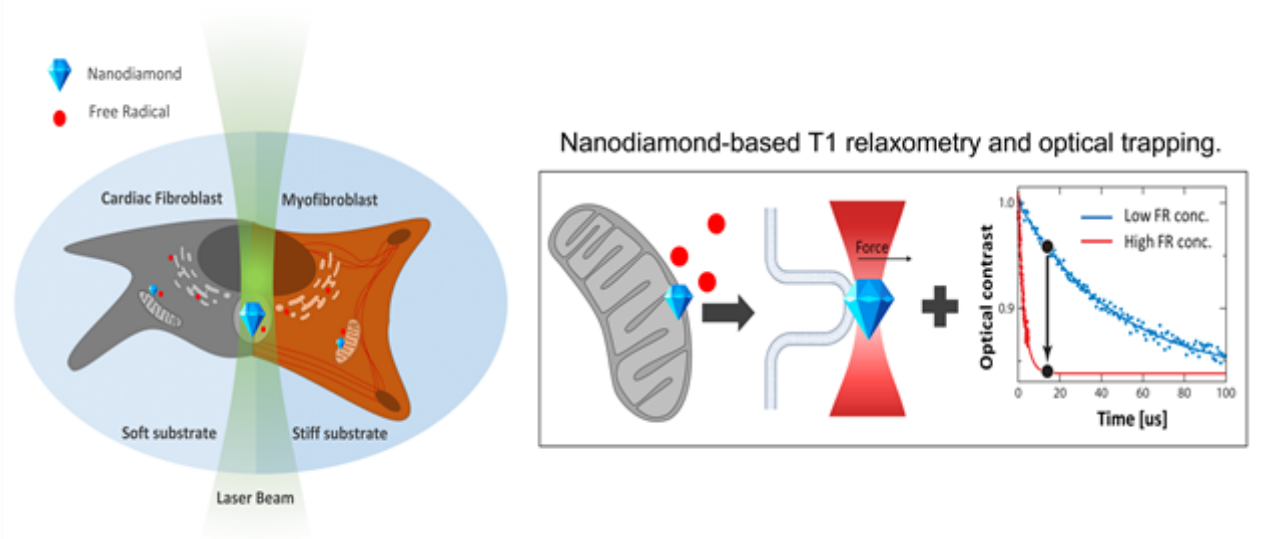

Keywords:

Quantum sensing, optical trapping, fibrosis

Reference:

1. Elías-Llumbet, Tian Y, Reyes-San-Martin C, Reina-Mahecha A, Damle V, Morita A, van der Veen HC, Sharma PK, Sandovici M, Mzyk A, Schirhagl R. Nano Letters 2023 23 (18), 8406-8410 doi: 10.1021/acs.nanolett.3c01506.
2. Kucsko G, Maurer PC, Yao NY, Kubo M, Noh HJ, Lo PK, Park H, Lukin MD. Nature 2013 1;500(7460):54-8, doi: 10.1038/nature12373.
3. Glenn DR, Bucher DB, Lee J, Lukin MD, Park H, Walsworth RL. Nature 2018, 555, 351–354, doi.org/10.1038/nature25781.
4. Miller BS, Bezinge L, Gliddon HD, Huang D, Dold G, Gray ER, Heaney J, Dobson PJ, Nastouli E, Morton JJL, McKendry RA. Nature2020, 587(7835):588-593, doi: 10.1038/s41586-020-2917-1.
5. Mzyk A, Sigaeva A, Schirhagl R. Accounts of Chemical Research 2022 55 (24), 3572-3580, doi: 10.1021/acs.accounts.2c00520.

920

Revealing the origin of green light emission in Cs4PbBr6 by cathodoluminescence

Tetsuya Kubota[1], Mr. Sotatsu Yanagimoto[1], Prof. Hikaru Saito[1,2], Dr. Keiichirou Akiba[1,3], Prof. Ayumi Ishii[4], Prof. Takumi Sannomiya[1]
[1]Tokyo Institute of Technology, Yokohama, Japan, [2]Kyushu University, Kasuga, Japan, [3]National Institute for Quantum Science and Technology (QST), Takasaki, Japan, [4]Waseda University, Shinjuku, Japan

PS-11, Lecture Theater 2, august 28, 2024, 14:00 - 16:00

Background
Metal halide perovskite is expected as next-generation material for the application for solar cells and light-emitting devices due to their excellent optical properties. Among them, Cs_4PbBr_6 has obtained significant attention as a luminescent material for its high-efficiency green emission and ease of synthesis. However, the mechanism of this green luminescence from Cs_4PbBr_6 has not been understood so far since the bandgap energy of Cs_4PbBr_6 lies in the ultraviolet range, which suggests that the green emission originates from intermediate states formed by impurities or defects within the host phase [1].
Previous discussions have proposed that $CsPbBr_3$ nanocrystals embedded in the Cs_4PbBr_6 host phase are the primary candidates for the green light source [1]. However, conventional photoluminescence measurements cannot spatially resolve such nanocrystals, and thus definitive evidence has been lacking. Recently, cathodoluminescence (CL) studies taking advantage of nanoscale spatial resolution achievable by electron excitation have reported the presence of microcrystals dispersed within the host phase [2]. However, detailed information of these microcrystals as well as their luminescence mechanism remains unclear, necessitating further elucidation of local optical properties.
In this study, we evaluated the nano-scale optical properties of Cs_4PbBr_6 powder samples using CL with scanning transmission electron microscopy (STEM). CL spectral and lifetime mapping analysis with a temperature dependence validated the inclusion of $CsPbBr_3$ nanoparticles within the Cs_4PbBr_6 host phase.

Methods
CL Measurement: Light emitted from the sample by electron irradiation was collimated by a parabolic mirror inside the microscope and directed toward the spectrometer for the CL spectrum measurement and a Hanbury Brown-Twiss (HBT) interferometer for the emission lifetime measurement. By the HBT measurement, one can measure emission lifetime without pulsing the electron beam. In these measurements, the light detection and electron beam scanning were synchronized, enabling CL spectral and lifetime mapping.
Sample Preparation: Cs_4PbBr_6 powder samples, were synthesized via a solution method. CsBr and $PbBr_2$ precursors were prepared and held in dimethyl sulfoxide (DMSO) for one hour. The precipitate, grown by the anti-solvent method, was washed with DMSO to obtain a powdered sample. X-ray diffraction (XRD) analysis confirmed only peaks corresponding to Cs_4PbBr_6 in the crystal structure.

Results
The secondary electron (SE) image of the measured powder is presented in Fig.(a). The CL image revealed the existence of bright spots with high luminescence intensity within the particle (Fig.(b)). Furthermore, the area-integrated spectrum showed peaks at emission wavelengths of 375nm, 520nm, and 700nm (referred to as Peak1, Peak2, and Broad Peak, respectively). According to previous studies, Peak1 is attributed to the optical transition of Pb ions originating from Cs_4PbBr_6 [3].

Broad peak can be attributed to emission derived from some other defects according to a radio-luminescence study by X-ray [4]. Peak2 is the green emission that we discuss in this study.
In the CL spectral mapping on the same measurement area that was conducted at low temperature (120K), the emission intensity of Peak1 exhibited a homogeneous distribution across the entire area, whereas Peak2 showed high intensity specifically in the bright spot regions (Fig.(c-d)). CL spectra were extracted from the region with single bright spot (Spot1), and regions without bright spots (Matrix), shown in Fig.(e). In all regions, the intensities of Peak1 and Broad Peak remained approximately the same, while the intensity of Peak2 changed depending on the presence of spots inside the signal extraction area in CL mapping (Fig.(d)). Particularly noteworthy is the significantly lower intensity of Peak2 in the Matrix region. On the basis of these findings, it is considered that nanoparticles forming the bright spots emit green light within the host phase of Cs_4PbBr_6.
To further investigate the optical properties of the green light emission, CL measurements were both performed at room temperature and low temperature (120K). It revealed that the emission wavelength is longer and the emission lifetime shorter at 120K than at room temperature. These trends are opposite to typical semiconductor materials but are consistent with $CsPbBr_3$ nanoparticles without a bulk host material [5]. This suggests that $CsPbBr_3$ nanoparticles surrounded by Cs_4PbBr_6 host phase are the origin of the highly effective green light emission.

Conclusions

In this study, we conducted nanoscale evaluation of the optical properties of Cs_4PbBr_6 using STEM-CL. By the spectral mapping, the presence of nanoparticles emitting green light within the Cs_4PbBr_6 host phase was observed. Furthermore, by measuring the spectra and lifetime under varying temperatures, it was confirmed that the characteristics of the green emission have the same tendency as bare $CsPbBr_3$ nanoparticles without a matrix. Thus, it is suggested that the highly effective green emission originates from $CsPbBr_3$ nanocrystals precipitated within the host Cs_4PbBr_6 material.

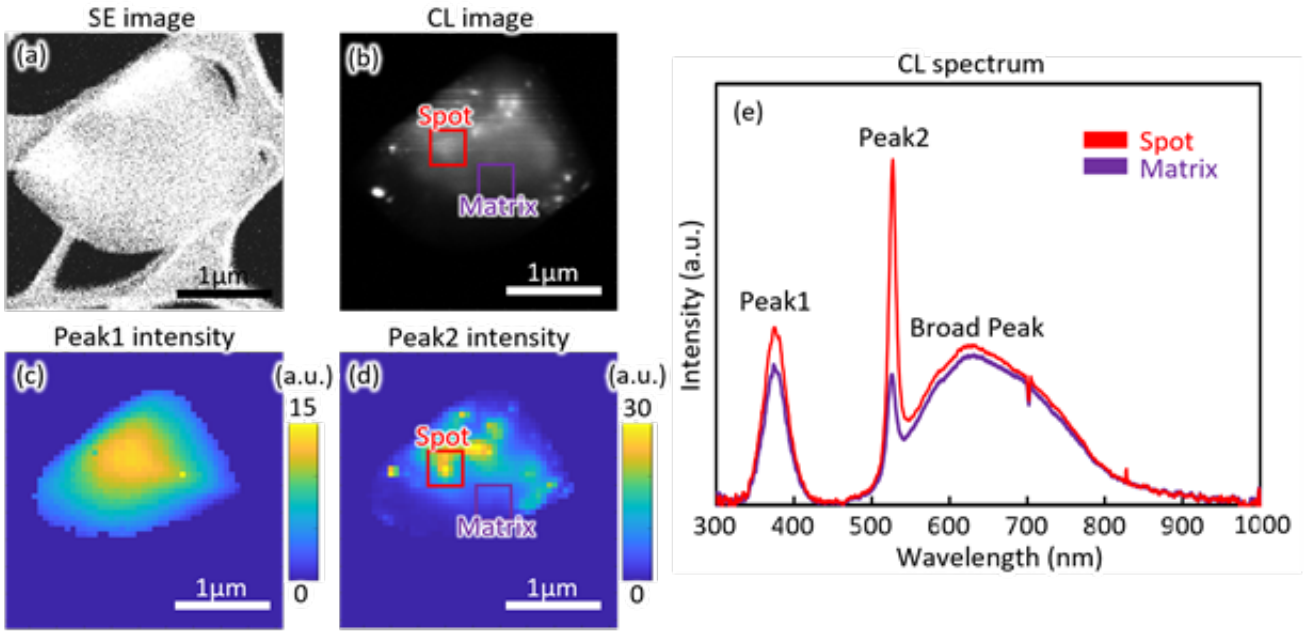

Keywords:

Cathodoluminescence
STEM
Perovskite
Lifetime

Reference:

[1] Q. Akkerman, Nano Lett., 17, 1924, (2017)
[2] T. Kubota, Appl. Phys. Express, 17, 015005 (2024)
[3] J. Yin, ACS Energy Lett., 2, 2805 (2017)
[4] Y. Li, Ceram. Int., 48, 16730 (2022)
[5] B. T. Diroll, Adv. Funct. Mater., 28, 1800945 (2018)

60

Unlocking Macroscale Solutions with Nanoscale Information: Towards Next-generation Optoelectronics

Prof Elke Debroye[1], Mr. Handong Jin[1], Mr. Amitrajit Mukherjee[1], Mr. Sudipta Seth[1], Mr. Johan Hofkens[1]
[1]KU Leuven, Department of Chemistry, Leuven, Belgium

Poster Group 2

Background incl. aims
Metal halide perovskites are a class of semiconductors that have garnered a tremendous amount of attention for application in optoelectronic devices. These low-cost materials exhibit outstanding properties, such as efficient light absorption, tunable emission, and good charge carrier transport. As an example, perovskites have accomplished a rapid rise in solar power conversion efficiency to over 25% in less than a decade, outperforming the conventional silicon solar cells. However, the fundamental understanding of their intrinsic properties and of the impact of defects on their photophysical performance and stability is lagging behind. We aim to exploit this nanoscale information to further improve the materials' applicability.
Methods and Results
Different synthesis strategies are applied to obtain perovskite nanocrystals with slight varieties in composition and structure. In this talk, I will focus on how we apply a set of advanced spectroscopic and correlated microscopic tools to detail the dynamics of the photogenerated charges and defects that govern the optoelectronic performance. Moreover, the stability of the corresponding materials will be discussed, and a novel approach to monitor device stability will be presented.
Conclusion
It will become clear that it is important to rationally micro-engineer the perovskites' chemistry, structure, and carrier dynamics toward an improved material platform for next-generation optoelectronics.

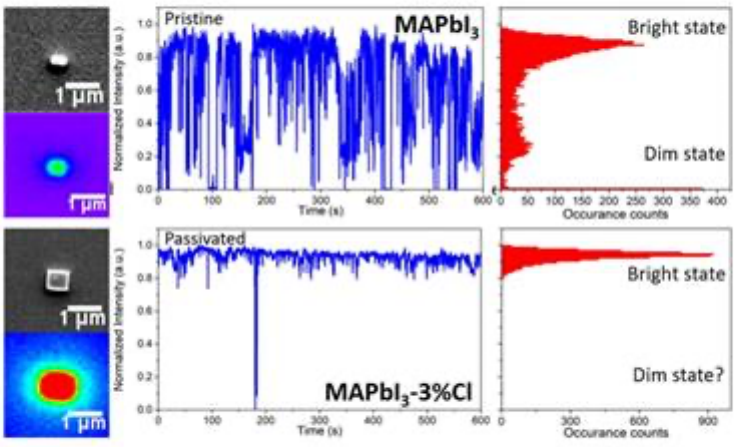

Keywords:

Hybrid perovskites, Correlated spectro-microscopy, Optoelectronics

Reference:

Jin, H.; Debroye, E.; et al. It's a Trap! Materials Horizons, 2020, 7, 397-410
Jin, H. et al. Chloride-Induced Trap Passivation in Lead Halide Perovskites. Adv. Optical Mater., 2021, 2002240
Jin, H.; Mukherjee, A.; et al. Single-particle optical study on chloride post-treatment of MAPbI3 nano/microcrystals. Nanoscale, 2023, 15, 5437-5447

89

Second harmonic generation microscopy of femtosecond microstructured crystals

Nuria Sevilla Sierra[1,2], Dr. Javier Rodríguez Vázquez de Aldana[1,2], Dr. Carolina Romero[1,2], Dr. Xavier Mateos[3], Dr. Ignacio Lopez-Quintas[1,2]
[1]Grupo de Investigación en Aplicaciones del Láser y Fotónica, Universidad de Salamanca (USAL), Salamanca, Spain, [2]Unidad de Excelencia en Luz y Materia Estructurada (LUMES), Universidad de Salamanca, Salamanca, Spain, [3]Física i Cristal·lografía de Materials (FiCMA), Universitat Rovira i Virgili (URV), Tarragona, Spain

Poster Group 2

Background incl. aims
Second Harmonic Generation (SHG) is a non-linear parametric optical process that implies the creation of one 2ω frequency photon while destroying two photons of frequency ω. It can only happen in non-centrosymmetric materials with non-vanishing second order susceptibility χ(2), such as anisotropic crystals or fibrillary microstructured biological tissues. There is a quadratic dependence of the SHG field with the fundamental ω one, which implies that the efficiency of the process increases with laser power, and thus, to generate measurable 2ω signals, ultrashort laser pulses are the most suitable sources. Second Harmonic Generation Microscopy (SHM) is a technique based on scanning the sample with a strongly focused ultrashort laser while measuring the SHG signal that is generated at each scanned position of the sample: since the main nonlinear laser-matter interaction is strongly restricted to the focal volume, the measurements are intrinsically confocal and therefore allow for precise 3D sectioning. The SHM technique can reveal rich morphological and structural information in the micro-scale, non-linear properties and/or different chemical composition of the sample.
Methods
Ultrashort femtosecond laser pulses can nano- and micro-structure transparent solids, locally modifying with high spatial precision their index of refraction. In this work we have investigated the non-linear response of two different previously micro-structured crystals: a non-centrosymmetric crystal (β-BaB2O4, BBO) and a centrosymmetric one (Nd:YAG). A femtosecond laser system (writing laser) was used to irradiate the sample in order to produce micro-modifications inside the crystal bulk. Different sets of irradiations were carried out both in BBO and Nd:YAG samples. A homemade microscopy set-up, able to operate as a conventional optical microscope and as a non-linear microscope, was used for the SHM measurements. In the non-linear mode of operation, the sample was illuminated with 120 fs laser pulses (measuring laser) with a central wavelength of 795 nm delivered by a Ti:Sapphire oscillator at a repetition rate of 80 MHz. For this study, SH maps were obtained by scanning the sample by moving the focusing point along the laser-inscribed tracks, which results in spatial variations of the signal intensity that can be measured and precisely assigned to their XYZ point of generation.
Results
BBO is one of the most widely used non-linear crystals due to its high optical non-linearity, wide range of transparency and physical robustness. It has the possibility to phase-match the SHG process in a large spectral window ensuring efficient conversion. In this work it was demonstrated that, under certain conditions, the SHG process in the damage tracks created by ultrashort laser irradiation exhibits a local enhancement in extraordinary polarization conditions. This phenomenon is attributed to a modification, achieved with the micro-structuring, of the effective non-linear coefficients of the susceptibility tensor, where irradiation modifies coefficients that take part in the extraordinary polarization conditions but not in the ordinary polarization situation. It can also be attributed to a

modification of the Gouy phase, because the irradiation and consequent breakage of symmetry in the crystals prevents phase compensation, thus allowing SHG signal to appear.
The second crystal studied, Nd:YAG, has a centrosymmetric structure. The generation of SH signal, localized at the damage tracks, was confirmed, and its features analyzed in detail in terms of the irradiation parameters of the inscribed micro-modifications. Findings show that the SH signal increases when increasing the inscription pulse energy, and when the scanning velocity is reduced (increased pulse overlap). It can be also seen that the measurement laser polarization has a significant effect on the intensity of the SHG signal.
The micro-modifications induced in the YAG structure by the laser irradiation explain the origin of this effects. These include a locally modified crystalline state (different inter-atomic distances; presence of lattice defects) and the formation of periodic structures or nanogratings in the amorphized region, along with phase transformation that can be found at the tracks. Due to the change in the inter-atomic distances in the dislocation surfaces or to a breakage of the inversion symmetry at the boundary between the crystal and the amorphous region, both, dislocations and the presence of an amorphized region, can be responsible for the generation of SH. In this case, the laser polarization for a more efficient SH signal is the one perpendicular to the interface, since it is the field orientation that probes the damage-induced anisotropy.
Conclusions
The observed nonlinear phenomena allow the use of SHM as a powerful technique for 3D imaging and diagnosing of photonic devices micro-structured by femtosecond lasers, such as optical waveguides or micrograting. Although the technique has been extensively employed in non-linear materials, these results open the possibility of waveguide or integrated photonic devices fabrication in centrosymmetric materials that are not initially expected to have a non-linear response.

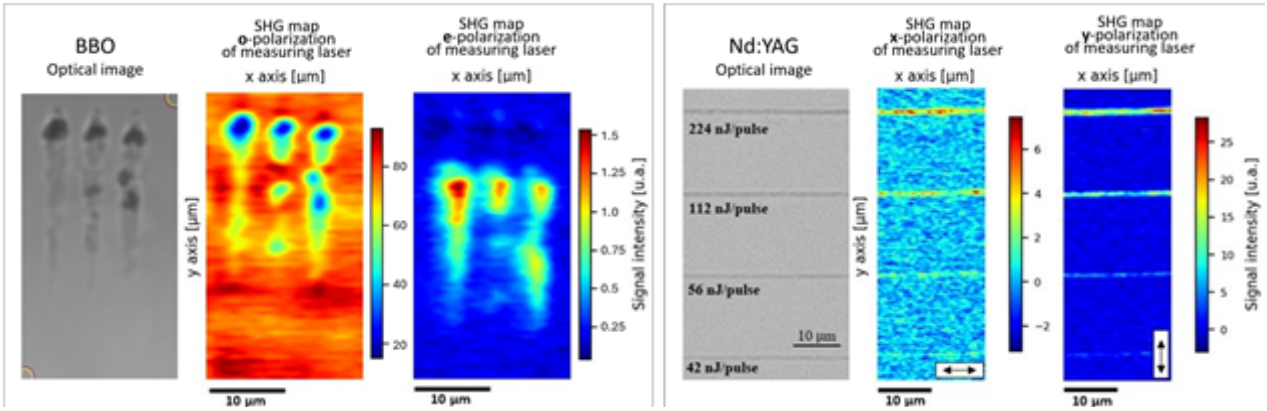

Keywords:

Nonlinear
Crystal
SHGMicroscopy
Microprocessing
Femtosecond

Reference:

- RW.Boyd. Nonlinear optics. Springer, 2008.
- DN.Nikogosyan. Beta barium borate (BBO) a review of its properties and applications. Applied Physics A, 52:359–368, 1991.
- SS.Fedotov et al. Plastic deformation as nature of femtosecond laser writing in YAG crystal. Scientific Reports, 10(1):19385, 2020.

174

Micro LED performance - a cathodoluminescence study

Mrs Névine Rochat[1], Palmerina González-Izquierdo[1], Davide Zoccarato[1], Fabian Rol[1], Julia Simon[1], Patrick Le Maitre[1], Marion Volpert[1], Matthew Charles[1], Matthieu Lafossas[1], Simona Torrengo[1], Noemie Bonnet[2], Toon Coenen[2], Lukasz Borowik[1]
[1]Univ. Grenoble Alpes, CEA, Leti, Grenoble, France, [2]DELMIC B.V, Delft, The netherlands

Poster Group 2

Background & aims
Gallium Nitride (GaN) microLEDs have received a lot of attention in the field of visible light microdisplays due to their interesting properties, such as high luminosity, wide wavelength range and robustness. However, their miniaturization poses a challenge due to the decrease of LED performance as the perimeter-to-surface ratio increases, a phenomenon that has not yet been fully understood. Studying carrier dynamics in these devices is crucial for understanding how recombination mechanisms affect their performance. The lateral diffusion length and carrier lifetime are therefore a major subject of interest for understanding and improving the characteristics of pixelated mesa LEDs.
In this work, we show the impact of Light Extraction Efficiency (LEE) and Internal Quantum Efficiency (IQE) independently as a function of mesa size and shape. Furthermore, lifetime measurements provide insights about the origin of IQE decrease near the mesa edge, showing the importance of diffusion coefficient and lifetime measurement techniques.
Methods
Multiple quantum well (MQW) LED structures (nGaN/5x(2.5nm InGaN/8nm GaN)/AlGaN EBL/pGaN) were patterned into 2.5, 5, 7.5 and 10 µm square and round mesas. These structures were analyzed using steady-state hyperspectral cathodoluminescence (CL) measurements at 10K and room temperature. The impact of mesa size and shape on LEE versus IQE has been explored. Additionally, Time Resolved Cathodoluminescence (TRCL) was performed with a streak camera at room temperature across a mesa to determine QW carrier lifetime and wavelength variation of the emitted light with the distance to the mesa edge.
Results
The maximum CL intensity at the center of the MQW mesas exhibits a non-monotonic trend with increasing mesa size, showing an optimal emission for the intermediate sized mesa of 7.5 µm, for both circular and square geometries. This behavior is explained by a competition between IQE (which decreases with mesa size reduction) and LEE (which increases with size reduction, with different trends for square and circular geometries), separated using the low and room temperature CL measurements. These results highlight the difficulty in properly interpreting CL intensity maps in terms of the impact of non-radiative recombination from the sides on LED mesa efficiency. However, the importance of IQE cartography at the nano scale to explore the impact of the mesa side remains significant. As already demonstrated in numerous papers, IQE decreases near the mesa wall. This decrease is mainly attributed to non-radiative recombination at the mesa edges and strongly affects smaller mesa performances. TRCL lifetime measurements across a mesa indeed show that carrier lifetime decreases near the mesa side. Furthermore, we observed a CL intensity reduction up to 3.5 µm from the mesa edge, which determines the optimal mesa size for emission. Thus, the diffusion length of carriers in the QW is one of the key parameters to minimize the impact of sidewall damage on LED efficiency. This means that a smaller diffusion length will reduce the impact of non-radiative recombination on the sidewalls on the LED efficiency.
Conclusion
This study investigates the influence of mesa size and geometry on external quantum efficiency, highlighting the significant impact of non-radiative recombination at the mesa edge. Moreover, a

competition between IQE and LEE is observed, elucidated through measurements at both low (10 K) and room temperature. This competition reveals an optimal LED size for two distinct mesa geometries, offering valuable insights for the design of microLED arrays. Furthermore, our findings provide clear indications for enhancing LED characteristics, such as mitigating surface recombination at sidewalls to reduce non-radiative recombination, or minimizing diffusion length to mitigate sidewall non-radiative impacts on small mesa sizes. Since diffusion length is intricately linked to the square root of the diffusion coefficient and radiative lifetime, characterizing the diffusion coefficient becomes critical. Both steady-state and time-resolved cathodoluminescence techniques are proposed to address these parameters effectively at the mesa scale.

This work, carried out on the Platform for Nanocharacterisation (PFNC), was supported by the “Recherche Technologique de Base” and "France 2030 - ANR-22-PEEL-0014" programs of the French National Research Agency (ANR). Manufacture of the samples was fund in the frame of the Important Project of Common European Interest (IPCEI) for microelectronics and as part of Nano 2022IPCEI.

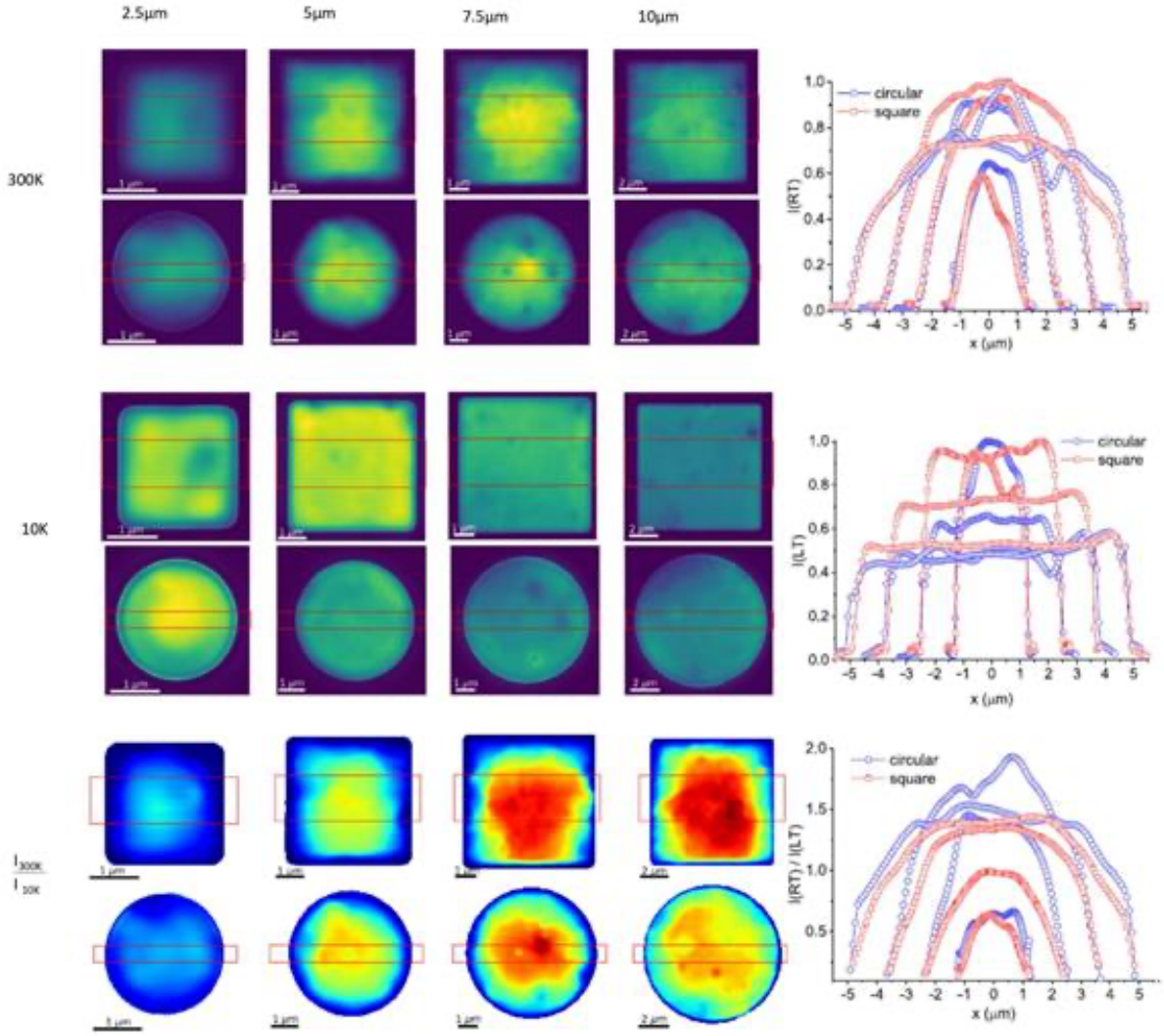

Integrated MQW CL intensity maps at 300K, 10K and I(300K)/I(10K) for four square and circular mesas with different widths (2.5, 5, 7.5, and 10 µm). Mesas of the same geometry are shown using the same color scale that covers the intensity range of the mesa showing the highest intensity value within the series. Right: Integrated MQW CL profile at 300K, 10K and I(300K)/I(10K), normalized to the highest value for each shape, and averaged in the vertical direction over the area marked as red rectangles in the maps, for four different sized square/circular mesas.

Keywords:

cathodoluminescence, quantum well, microLED

Reference:

P. González-Izquierdo et al, Influence of Shape and Size on GaN/InGaN µLED Light Emission: A Competition between Sidewall Defects and Light Extraction Efficiency. ACS Photonics 2023, 10, 4031−4037

S. Finot et al, Surface Recombinations in III-Nitride Micro-LEDs Probed by Photon-Correlation Cathodoluminescence. ACS Photonics 2022, 9 (1), 173–178

384

Electron beam imaging of extremely confined optical modes in topology-optimized dielectric photonic cavities

Dr. Michael Seifner[1,2], M.Sc. Ali Babar[2,3], B.Sc. Anne Sofie Darket[2,3], Assistant Professor Babak Vosoughi Lahijani[2,3], Associate Professor Rasmus Christiansen[2,4], Senior Researcher Elizaveta Semenova[2,3], Professor Søren Stobbe[2,3], Senior Researcher Philip Kristensen[2,3], Senior Researcher Shima Kadkhodazadeh[1,2]
[1]DTU Nanolab, Technical University of Denmark, Kongens Lyngby, Denmark, [2]NanoPhoton - Center for Nanophotonics, Technical University of Denmark, Kongens Lyngby, Denmark, [3]DTU Electro, Technical University of Denmark, Kongens Lyngby, Denmark, [4]DTU Construct, Technical University of Denmark, Kongens Lyngby, Denmark

Poster Group 2

Background incl. aims
Dielectric photonic cavities can store light efficiently and have proven capable of spatially confining light far below the diffraction limit, making them promising building blocks for integrating photonics and electronics.[1] The small mode volumes realized in these structures reveal the limitations in spatially resolving the optical modes by conventional optical characterization techniques. In comparison, transmission electron microscopy (TEM) can reach sub-nanometer spatial resolutions, making this technique attractive for characterizing nanophotonic structures.[2] In particular, the swift electrons in an electron microscope can couple to the optical modes of nanostructures, leading to electron energy losses.[3] The electron's energy loss can be measured by electron energy loss spectroscopy (EELS) with high spatial resolution when combined with scanning transmission electron microscopy (STEM). This contribution aims to visualize the fundamental mode at 1550 nm wavelength of a topology-optimized photonic cavity with extreme dielectric confinement (EDC).
Methods
Si-based dielectric photonic cavities are designed by an inverse design process using topology optimization and are subsequently fabricated by dry etching techniques in the cleanroom.[1, 4] The dielectric photonic structures are lifted out individually from the substrate using a plasma focused ion beam (PFIB)/scanning electron microscope (SEM) and attached to a TEM-compatible grid. The lifted out cavities are examined using a Thermofisher TEM instrument equipped with a monochromator and an aberration corrector, giving energy and spatial resolutions better than 0.1 eV and 0.2 nm, respectively. EELS spectrum images are acquired at various sample tilt angles, revealing information about the optical modes' evolution in space. The EEL spectra are analyzed using different fitting approaches after a Richardson-Lucy deconvolution of the zero loss peak to produce the electron energy loss maps for the mode of interest at approximately 0.80 eV. EEL spectra are simulated using a quasinormal mode expansion of the electromagnetic Green tensor to facilitate a detailed analysis of the experimental data.[5]
Results
STEM images acquired in the tilt range 0°-90° show the structure of the dielectric photonic cavity used for the present study (Figure, panel a). EEL spectrum images acquired for each tilt angle reveal the excitation of different cavity modes, with the fundamental mode at 0.80 eV being most strongly excited at the highest tilt angle, which is visualized by EELS intensity maps (Figure, panel b) and sum spectra from the bowtie region of the photonic cavity (Figure, panel c). This observation agrees well with the simulations and is caused by the in-plane polarization of this mode tailored by the inverse design process. EELS intensity maps of this mode confirm its tight confinement in the center bridge of the bowtie of the cavity structure. Besides the fundamental mode, additional optical modes with different energies, polarizations, and spatial confinements are observed. The simulated EEL spectra for different sample positions agree very well with the experimental results.

Conclusions

The results of this contribution showcase the application of EELS in nanoscale imaging of optical modes in dielectric photonic cavities and its potential for gaining deeper insights into light's interaction with matter and confinement at deep sub-wavelength dimensions.

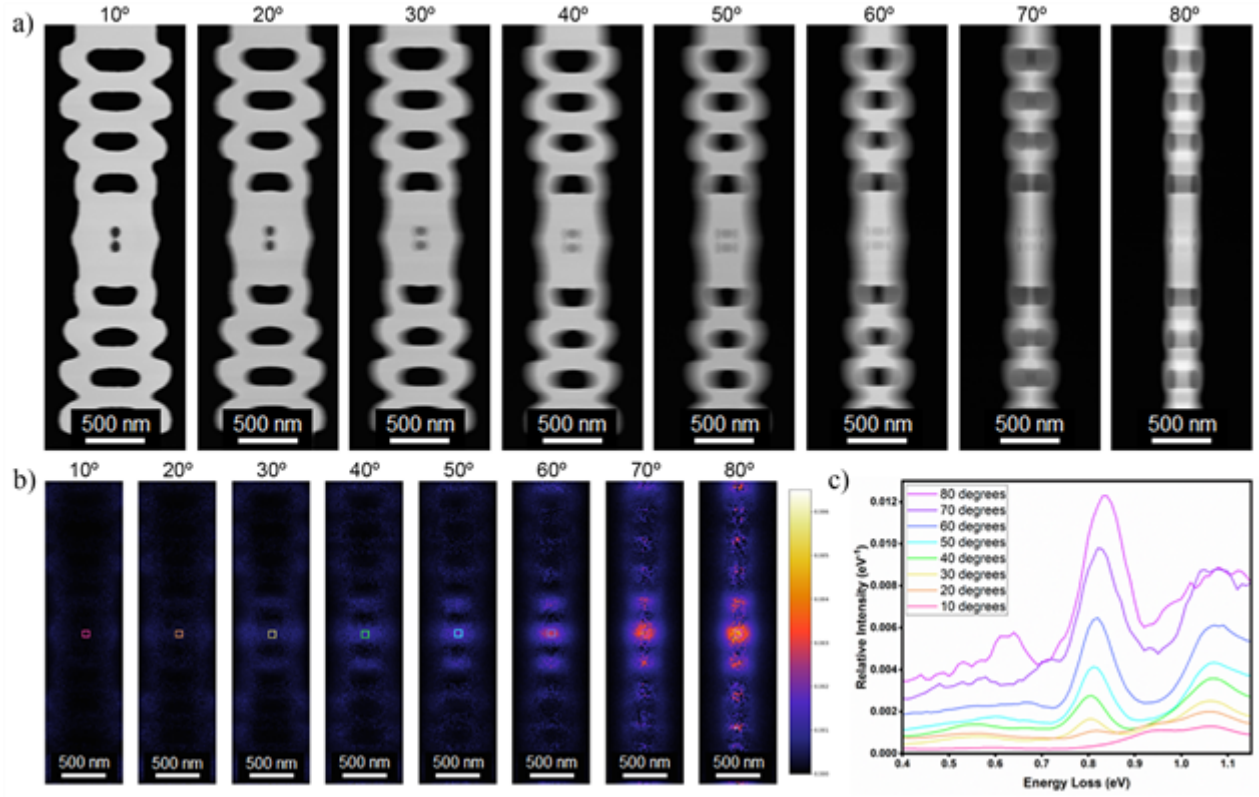

Keywords:

STEM, EELS, nanophotonics, photonic cavities

Reference:

1) M. Albrechtsen, B. Vosoughi Lahijani, R. E. Christiansen, V. T. H. Nguyen, L. N. Casses, S. E. Hansen, N. Stenger, O. Sigmund, H. Jansen, J. Mørk, S. Stobbe, Nat. Commun., 13 (2022)
2) A. Polman, M. Kociak, F. J. García de Abajo, Nat. Mater., 18 (2019)
3) F. J. García de Abajo, M. Kociak, Phys. Rev. Lett., 100 (2008)
4) R. E. Christiansen, O. Sigmund, J. Opt. Soc. Am. B, 38 (2021)
5) R.-C. Ge, S. Hughes, J. Opt., 18 (2016)

429

Fabrication of 2-dimensional disordered assemblies of gold nanoparticles and investigation of localized surface plasmon resonances

Kristina Weinel[1,2], Dr. Johannes Schultz[1], Mohammed Fayis Kalady[1], Dr. Daniel Wolf[1], Dr. Leonardo Agudo Jácome[2], Prof. Dr. Axel Lubk[1]
[1]Leibniz-Institut for Solid State and Materials Research Dresden, Dresden, Germany, [2]Federal Institute for Materials Research and Testing, Berlin, Germany

Poster Group 2

Background incl. aims
Interaction of electromagnetic waves, such as electron beams or light, with conductive material can lead to localized surface plasmon resonances (LSPRs) where the incoming energy can be deposited in a collective excitation of electrons of the conduction band, which in turn can result in coherent localized plasmon oscillations. LSPR in metallic nanostructures, such as nanoparticles (NPs), which are sensitive to geometry, material composition and environment, are currently utilized in a wide range of applications, such as surface-enhanced Raman spectroscopy, plasmonic wave guides, improved solar cells, on-chip particle accelerators and nanoantennas. A host of studies that focus on plasmonic NPs ranging from single NPs with several shapes (cubic, spherical, tetrahedral) over 1D assemblies of NPs such as chains [1], to ordered 2D assemblies of NPs [2] show an increase of the complexity regarding the hybridization behavior of LSPRs eventually lead to delocalized Surface Plasmons. Furthermore, Anderson predicted in 1977 [3] the absence of diffusion or delocalization of waves in disordered systems, which has been discussed as the underlying mechanism for LSPRs localization in disordered metallic thin films and ultrathin 2D networks [4]. Our aim is to further develop these studies on the surface plasmon localization in disordered structures by (1) developing a novel NPs assembly fabrication method that allows fabricating disordered assemblies of NPs of a wide range of NPs sizes, and (2) probing the LSPR with high-resolution electron energy-loss spectroscopy (EELS). Moreover, the dominant dipolar interaction between the NPs, also facilitates an efficient numerical modeling of these systems, which in comparison with the experiments allows for an in-depth study of the impact of various geometric parameters as well as retardation and life-time damping on the observed localization behavior.

Methods
To synthesize 2D disordered assemblies of gold NPs on a TEM transparent silicon oxide substrate, a new synthesis routine was developed. This procedure is based on sublimation and redeposition of a gold microparticle precursor induced by an electron beam in a scanning electron microscope (SEM) operated at 30 kV. To characterize the assembly of synthesized NPs in terms of size, shape and spreading over the substrate, TEM measurements were conducted subsequently. To study LSPRs experimentally, EELS in scanning transmission electron microscopy (STEM) mode was carried out. The numerical modelling of LSPRs was performed using a self-consistent dipole model.

Results
The synthesized 2D disordered gold NPs assemblies (see Fig. 1a) exhibit a gradient in the NPs mean size, which ranges from 100 nm close to the precursor location down to 2 nm at a distance of more than 20 µm from the precursor location. Additionally, the interparticle distance between the gold NPs increases with increasing distance to the precursor location.
The experimental investigation (see Fig. 1b) as well as the numerical simulation (see Fig. 1c) of the LSPRs demonstrate a localization behavior that decreases toward larger energies, which is driven by the disorder of the NPs assembly (mainly the random particle distance). That localization behavior stays in contrast to what was found in ultrathin 2D gold networks showing increasing of localization

towards higher LSPRs energies. By varying the geometric parameters of the NPs assembly in the simulation, we could identify the NPs thickness as the parameter, that determines the energy-dependence of the localization. Specifically, a critical thickness of approx. 10 nm separates the two localization regimes, which correlates to the energy of the dipole mode resonance crucially depending on the thickness of the NPs.

Conclusion

2D disordered assemblies of gold NPs of a wide range of NPs sizes and distances can be synthesized directly on thin substrates facilitating structural characterization and EELS measurements in a TEM. It could be shown that such assemblies exhibit LSPRs with a localization behavior that may be tuned by the NPs sizes (including thickness) and interparticle distances. The proposed synthesis of random NPs assemblies opens new avenues for fundamental studies on Anderson localization in disordered plasmonic structures as well as its applications such as surface-enhanced Raman spectroscopy where localization behavior must be tuned to specific wave lengths.

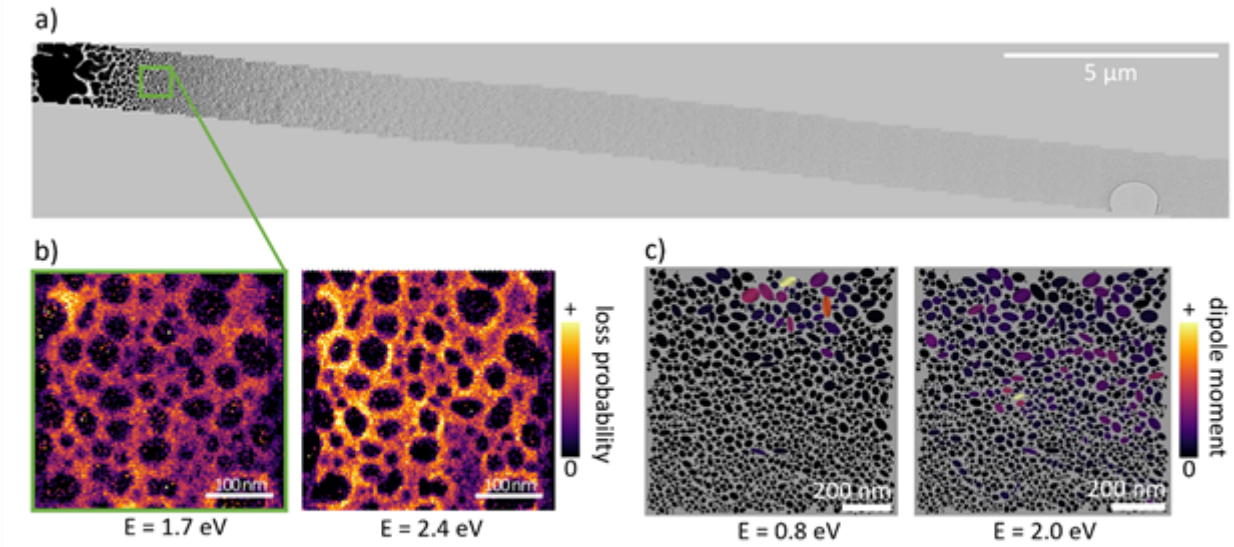

Figure 1 a) Stitched bright-field TEM images showing the disordered assembly of gold NPs over several tens of micrometers. b) LSPR maps obtained by STEM spectrum imaging at energy losses of E=1.7 eV and E=2.4 eV. c) Simulated LSPR maps derived from a self-consistent dipole model.

Keywords:

SEM, TEM, LSPR, Au-NPs-Synthesis, Disordered-Assemblies

Reference:

[1] Martin Mayer et al., “Direct Observation of Plasmon Band Formation and Delocalization in Quasi-Infinite Nanoparticle Chains”, doi: 10.1021/acs.nanolett.9b01031, 2019
[2] Humphrey, Alastair D. and Barnes, William L., "Plasmonic surface lattice resonances on arrays of different lattice symmetry," Physical Review B 90, 075404 (2014)
[3] A. Lagendijk, B. v. Tiggelen, and D. S. Wiersma, “Fifty years of Anderson localization,” Physics Today 62, 24–29 (2009)
[4] Johannes Schultz et al., “Maximal Anderson Localization and Suppression of Surface Plasmons in Two-Dimensional Random Au Networks”, arXiv preprint arXiv:2107.06616, 2021

566

Simulating electron energy-loss spectroscopy and cathodoluminescence for nanoparticles located on substrates

Alexander Kichigin[1], Mingjian Wu[1], Stefanie Rechberger[1], Benjamin Apeleo Zubiri[1], Maxim Yurkin[2], Erdmann Spiecker[1]
[1]Institute of Micro- and Nanostructure Research (IMN) & Center for Nanoanalysis and Electron Microscopy (CENEM), Friedrich-Alexander-Universität Erlangen-Nürnberg, IZNF, Erlangen, Germany, [2]CNRS, INSA Rouen Normandie, Univ Rouen Normandie, Normandie Univ, CORIA UMR 6614, Rouen, France

Poster Group 2

Background
Electron energy-loss spectroscopy (EELS) and cathodoluminescence (CL) are widely used to study the plasmonic properties of individual nanoparticles. In the experiment, the sample is irradiated with relativistic electrons having energy of about 100 keV. After the interaction with the sample, electrons' energies are measured to obtain the energy loss spectrum (EELS spectrum). When interacting, the sample itself begins to emit photons. This light is collected by a parabolic mirror to obtain CL spectrum. The main advantage of EELS/CL over light scattering methods is the ability to study plasmonic properties with a spatial resolution of less than 1 nm (at wavelengths of visible light and infra-red).

Methods
We extended the capabilities of the discrete dipole approximation (DDA) to simulate EELS and CL. Until recently, there was only a theory for simulating the case of particles located in vacuum, which is never true in the experiment. In an electron microscope, the particle is always placed inside or on top of the substrate medium, which redshifts the plasmonic response of the sample. We extended our previously published DDA theory for particles inside an infinite medium[1] to simulate EELS and CL for particles on top of a semi-infinite medium, which successfully reproduces experimental results for particles deposited on TEM membranes of finite thickness.

Results
With the extended theory, the simulations successfully reproduce the results of EELS experiment where a gold nanoprism (209 nm side length, 10 nm thickness) was deposited on 30-nm-thick Si3N4 substrate.[2] A straightforward workaround for such simulations (with any DDA code) is to discretize a finite volume of the substrate below the particle, which would take 1 645 070 dipoles for both prism and the substrate (Fig. 1a), making it a heavy computational task. In the extended theory, however, the presence of substrate is accounted in the DDA formulation of the problem (by adjusting the dipole-dipole interaction function) requiring only 66 206 dipoles to discretize only the prism itself (Fig. 1b). This requires much less computational resources, leading to about 10 times faster simulations.
In the simulations of the prism, the Si3N4 refractive index was set to a constant 2.15 for all energies, and the refractive index of gold was taken from the data by Babar et al.[3] The redshift caused by the semi-infinite substrate in the simulated plasmon energy peaks matches the ones observed in the experiment by Griffin et al.[2]. Moreover, the simulated plasmon maps (Fig. 1c) also match the experimental ones,[2] in contrast to the simulations for a particle in vacuum in that paper.
The extended theory also successfully reproduces the CL experiment where a gold nanorod was placed on top of SiO2 membrane,[4] and even the CL experiment where a gold nanorod-shaped antenna was on top of gold substrate.[5]

Conclusion

Simulations with the semi-infinite substrate theory successfully reproduce experimental spectra and plasmon maps for both EELS and CL for samples on top of dielectric substrates, and for CL even in the case of a metallic substrate. Brief theory overview followed by simulation results in comparison with previously published and our own experiments will be presented at the conference.

Acknowledgements

The authors gratefully acknowledge financial support by the DFG via the Collaborative Research Centre SFB 1411 (Project-ID 416229255).

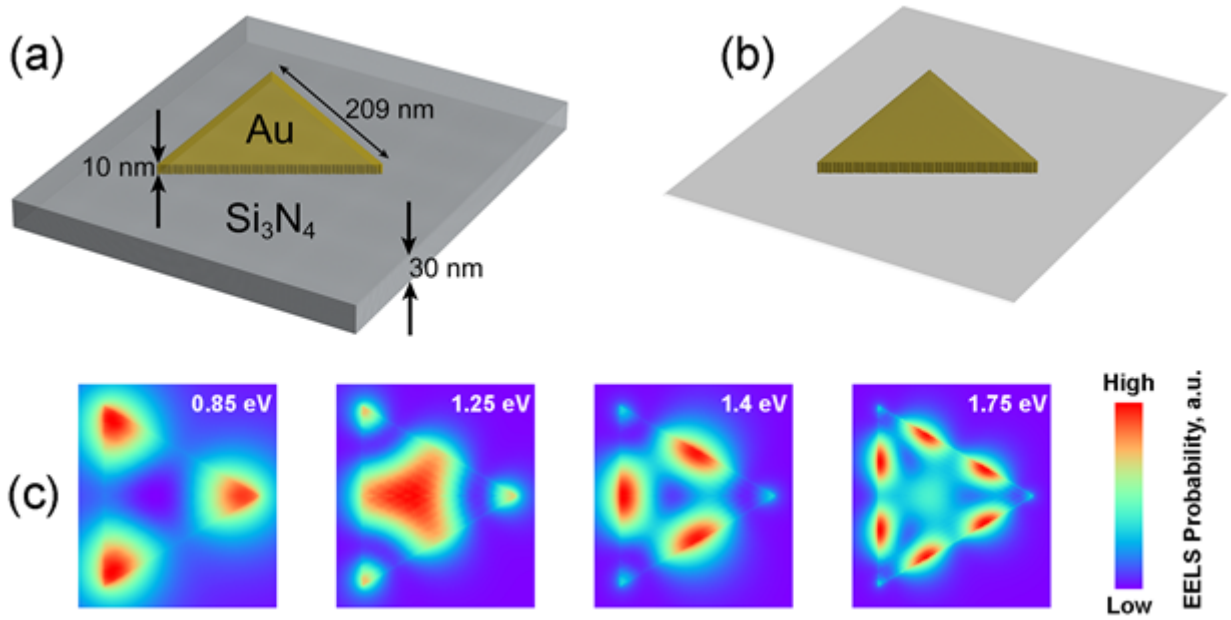

Keywords:

Plasmonics, EELS, cathodoluminescence, DDA

Reference:

[1] A. A. Kichigin, M. A. Yurkin, J. Phys. Chem. C 2023, 127, 4154.
[2] S. Griffin, N. P. Montoni, G. Li, P. J. Straney, J. E. Millstone, D. J. Masiello, J. P. Camden, J. Phys. Chem. Lett. 2016, 7, 3825.
[3] S. Babar, J. H. Weaver, Appl. Opt. 2015, 54, 477.
[4] J. K. Day, N. Large, P. Nordlander, N. J. Halas, Nano Lett. 2015, 15, 1324.
[5] T. Coenen, E. J. R. Vesseur, A. Polman, ACS Nano 2012, 6, 1742.

605

Creating free-standing nanostructures with plasmonic properties via Focused Electron Beam Induced Deposition

Di Di Verena Reisecker[1], David Kuhness[1,2], Georg Haberfehlner[1,3], Michele Brugger-Hatzl[3], Robert Winkler[1,2], Anna Weitzer[1], David Loibner[1,2], Martina Dienstleder[3], Gerald Kothleitner[1,3], Harald Plank[1,2,3]
[1]Institute of Electron Microscopy and Nanoanalysis (FELMI), Graz University of Technology, Graz, Austria, [2]Christian Doppler Laboratory DEFINE, FELMI, Graz University of Technology, Graz, Austria, [3]Graz Centre of Electron Microscopy (ZFE), Graz, Austria

Poster Group 2

Over the past decades, significant interest was directed towards the optical properties of nanoscale structures. As they are highly sensitive to slight changes in material, geometry, size and arrangement, controlling these aspects in every detail allows to tailor their plasmonic response according to the targeted operation and opens up access to a multitude of applications in research and development. With miniaturization reaching its limits, expanding the nanostructures into the third dimension could give access to horizontal and vertical mode coupling, reduce substrate damping, increase device performances and allow for the investigation of novel optical effects. Herein, we present how Focused Electron Beam Induced Deposition (FEBID), a 3D manufacturing technique capable of printing nanostructures with feature sizes down to around 10 nm, can be applied to fabricate and tune the plasmonic properties of planar and free-standing gold nanostructures.[1] Therefore, planar gold nanowires as well as free-standing nanotips of varying geometries are printed and purified with a focused electron beam and their plasmonic response investigated through STEM-EELS mapping measurements. Corresponding plasmon simulations provide additional backing to our experimental discoveries, displaying excellent agreement (see Figure 1). This study lays the foundation for on-demand spectral tuning of the plasmonic response in 3D systems through upfront modeling and design of tailored nanostructures, thereby unlocking opportunities for innovative plasmonic applications in 3D space.

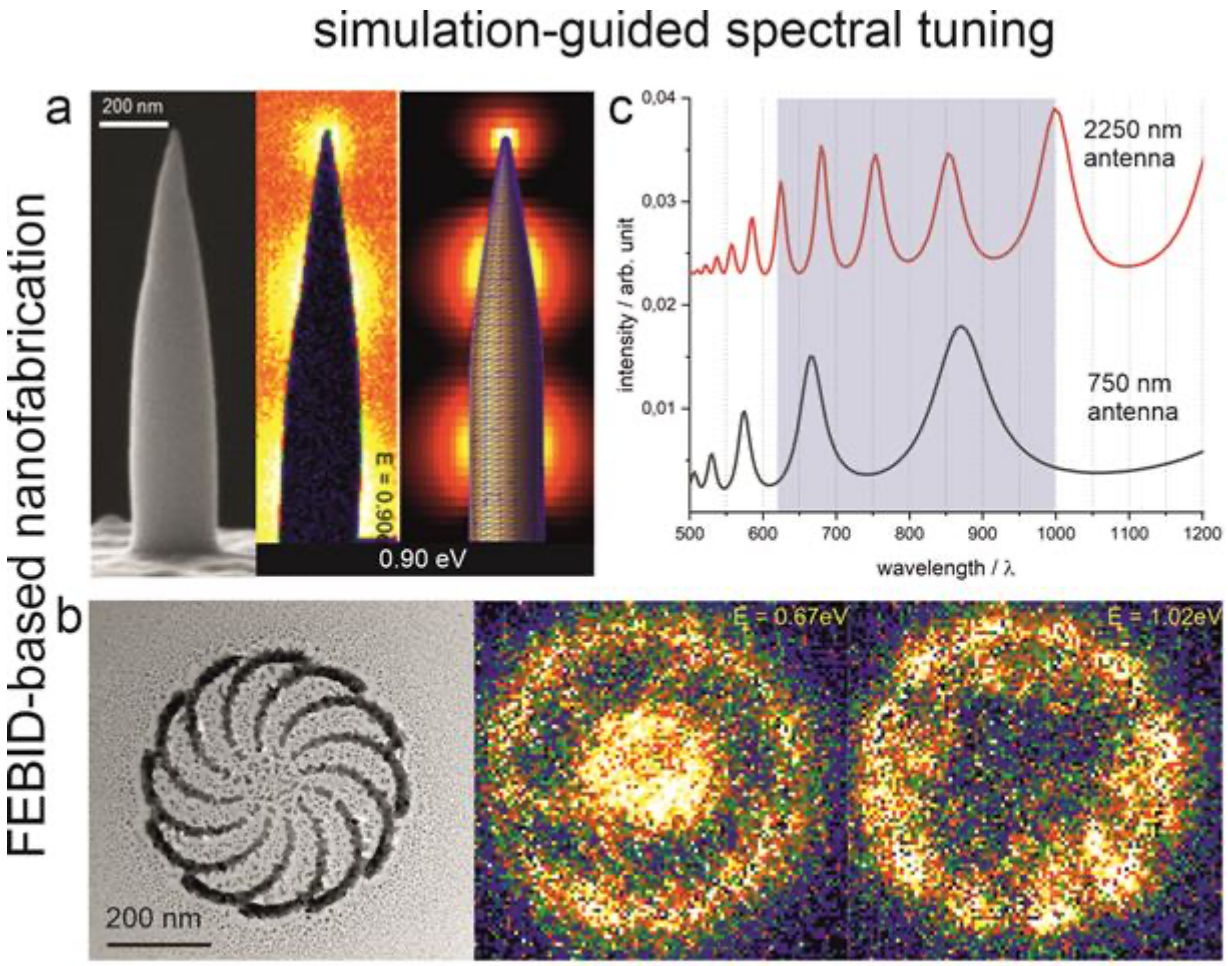

Figure 1: Free-standing nanotip **(a)** and planar spiral structure **(b)** fabricated with FEBID and purified via electron beam irradiation in water vapor atmosphere along with experimental and simulated EELS maps at selected energies. **(c)** Spectral tuning is exemplarily shown for the free-standing nanotip exhibiting a height of either 2250 nm or 750 nm.[1]

Keywords:

Nanoplasmonics, Spectral Tuning, Additive Manufacturing,

Reference:

[1] V. Reisecker, D. Kuhness, G. Haberfehlner, M. Brugger-Hatzl, R. Winkler, A. Weitzer, D. Loibner, M. Dienstleder, G. Kothleitner, H. Plank, Adv. Funct. Mater. 2023.

837

Control of inter-particle distance between nanoparticles using DNA origami

Jannik Guckel[1,2], Dr Daesung Park[1,2], Dr Markus Etzkorn[2,3], Zhe Liu[2,3], Zunhao Wang[1,2], Dr. Birka Lalkens[2,4]
[1]Physikalisch-Technische Bundesanstalt, Braunschweig, Germany, [2]Laboratory for Emerging Nanometrology (LENA), Braunschweig, Germany, [3]Institute of Applied Physics, Technische Universität Braunschweig, Braunschweig, Germany, [4]Institute of Semiconductor Technology, Technische Universität Braunschweig, Braunschweig, Germany

Poster Group 2

Background incl. aims
Metallic nanoparticle pairs, known as dimers, have been used to enhance the excitation rate of single quantum emitters. Among other parameters, the inter-particle distance (d) has crucial impact on the electro-magnetic field around the particles, leading to enhancement of signals. Thus, precisely controlling d is desired for achieving the optimized performance for the given applications. Usually, d is controlled by using linker molecules. In this study, we alternatively utilized the DNA strands to control d. Since this technique has several independent parameters, it ensures a high degree of customization.
Methods
The synthesis of dimers was adapted by Gür et. al. [1] and consists of 2 steps. In the first step, we functionalized the nanoparticles using using single strands of poly-thymine. In the second step, selected staples of the DNA origami were extended with pieces of single-stranded poly-adenine. The complementary strands connect via hydrogen bonding, forming the strand of length (L) (Fig. 1A). We analyzed multiple secondary electron (SE) images of these self-assembled gold dimers using different L from different samples in order to verify the reliability of the control of d. Based on geometric considerations (Fig. 1B), we expect an increase in the standard deviation σ of d. We therefore required large amount of dimers to obtain statistical significance. The detailed analysis of the SE images was achieved by using a novel analysis tool developed for this task. The tool uses the intensity thresholding technique to segregate the DNA origami from the silicon wafer, and then analyzes each origami individually. We use circle Hough transform (CHT) to detect the spherical particles, with a set of novel classification routines to assign one of 4 classes (monomer, dimer, single particle on wafer, agglomerate) to each particle (Fig. 2)
Results
We analyzed the distribution of d across multiple samples using our tool, measuring more than one thousand dimers per sample. While the general trend of σ increasing with L could be observed in the experimental data, the proposed effect of L on σ is smaller than expected (Fig. 3). The deviation between the simulation and experiment can be attributed to our model only taking sample geometry with few assumptions about the DNA strands into account. However, based on our observations, more complex effects of DNA bonding and the interactions between nanoparticles, DNA strands and DNA origami led to notable change in the distribution of d. Therefore, an accurate prediction of the distribution of d requires a more complex model.
Conclusions
We investigated multiple samples, in which the different inter-particle distances of gold dimers were achieved using different DNA strand length on the DNA origamies. Based on sample geometry, we expected a significant effect of the DNA strand length on the distribution of d, with longer strands resulting in a broader distribution. Our experiments confirm the existence of this trend, even though the effect is smaller than our initial expectations. Our results show that complex interactions within the material system have significant effects on the distribution of d, making an accurate prediction of the distribution more complex than anticipated.

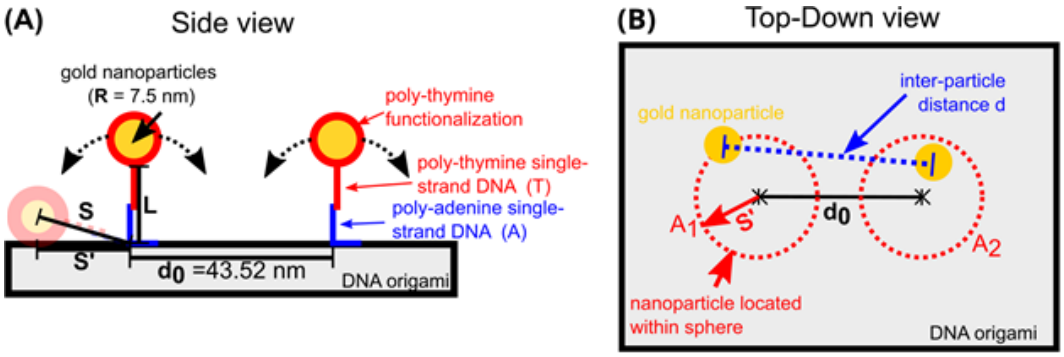

Fig. 1: Connection between gold nanoparticles and DNA origami: (A) The connecting DNA strand results from hydrogen bonding between a poly-thymine and poly-adenine DNA strand, and (B) The inter-particle distance d is assumed as the center-to-center distance between both nanoparticles in top-down view. We expect both particles to be randomly distributed within S' from their anchor point. As S' increases with L, we expect an increase in σ.

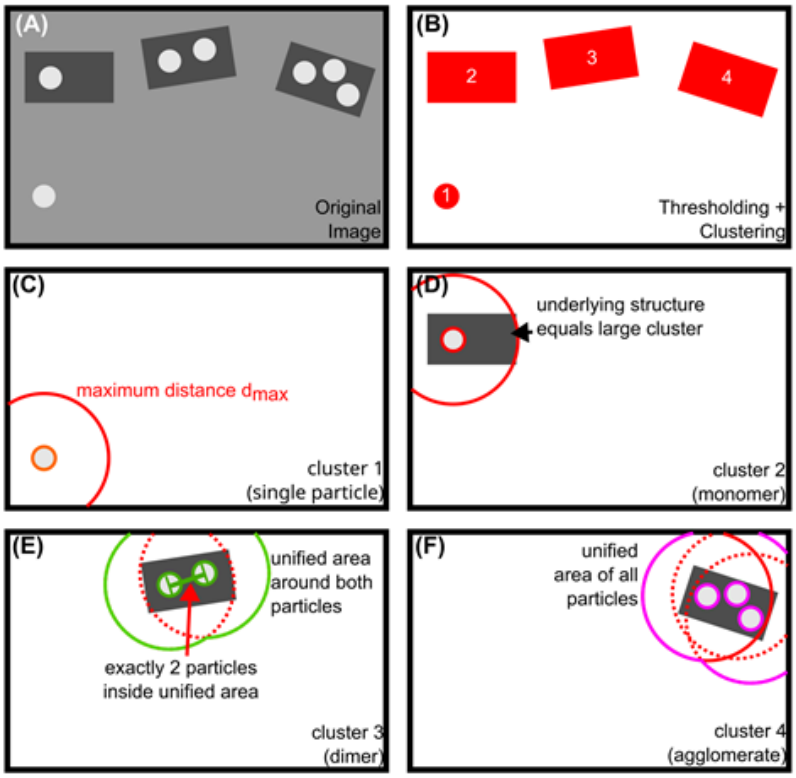

Fig. 2: Workflow of the analysis tool: (A) a sketch of nanostructures on a water, (B) segregation of nano-structures by thresholding and grouping of pixel clusters. Each structure is then analyzed individually. (C)-(F) example for each particle class: single particles and monomers have no particle within d_{max}, the maximum value of d based on sample geometry. Dimers are pairs of nanoparticles on the same origami without additional partner options within their d_{max}. Agglomerates are groups of particles with unclear partner relationship. The particle classes are assigned based on the number of other particles in their vicinity with additional criteria.

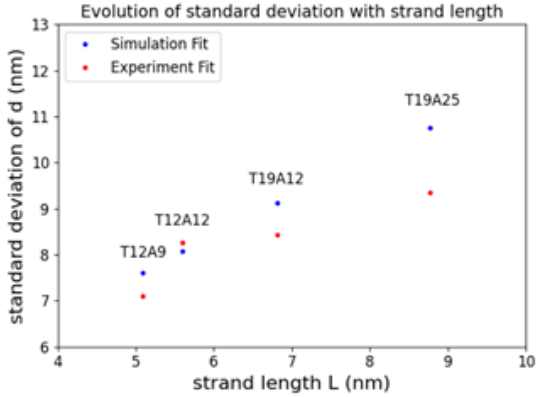

Fig. 3: Correlation between the strand length L and the standard deviation σ. In general, the effects of L were overestimated in the simulation. The samples are named by the number of base pairs in their respective poly-thymine and poly-adenine strands, with higher numbers resulting in a longer strand.

Keywords:

gold dimers, DNA origami

Reference:

Gür, F. N.; Schwarz, F. W.; Ye, J.; Diez, S.; Schmidt, T. L. (2016) Toward Self-Assembled Plasmonic Devices: High-Yield Arrangement of Gold Nanoparticles on DNA Origami Templates. ACS Nano, 10 (5), 5374–5382.

849

Influence of the deposition parameters on properties of gold plasmonic antennas

Michael Foltýn[1], Marek Patočka[1], Rostislav Řepa[1], Tomáš Šikola[1], Michal Horák[1]
[1]Brno University of Technology, Brno, Czech Republic

Poster Group 2

The properties of plasmonic antennas depend on a variety of factors, including the antenna size, shape, and material. Although gold plasmonic antennas have been studied extensively over the last few years, the influence of parameters used for gold thin film deposition on the resulting plasmonic behaviour of fabricated antennas remains unexplored.
We deposited gold films with thicknesses of 20 nm, 30 nm, and 40 nm at various deposition rates by an ion-beam-assisted deposition. We analysed the structure of deposited films by X ray diffraction and transmission electron microscopy. We fabricated gold plasmonic antennas by FIB lithography [1, 2] and evaluated the ease of fabrication for each deposited layer used, based on the fabrication yield of three antenna types. Further on, we studied the plasmonic behaviour of fabricated antennas by EELS [3] and compared the plasmon resonance intensity and Q factors of individual antennas.
Our results [4] show, that for fabrication of plasmonic antennas by FIB lithography, the films deposited at 0.3 nm/s are optimal, as the fabrication yields of these layers are the highest. However, in terms of plasmonic properties, antennas fabricated from 20- and 30-nm thick layers deposited at 0.1 nm/s exhibit the highest plasmon resonance intensity and highest Q factors. In the case of 40 nm thick layers, the best plasmonic performance is achieved in antennas fabricated out of gold films deposited at 0.3 nm/s. Figure below shows the results for 30-nm-thick gold layer: fabrication yield (A), EEL spectra for two specific electron beam positions at the corners (B) and in the gap (C) of a bowtie antenna, and Q factros of the transverse dipole (TD) and longitudinal dipole (LD) mode (D).
This study sheds light on the interplay between gold thin film deposition parameters and the resultant plasmonic behaviour of antennas, offering valuable recommendations for optimizing the fabrication process of plasmonic devices.

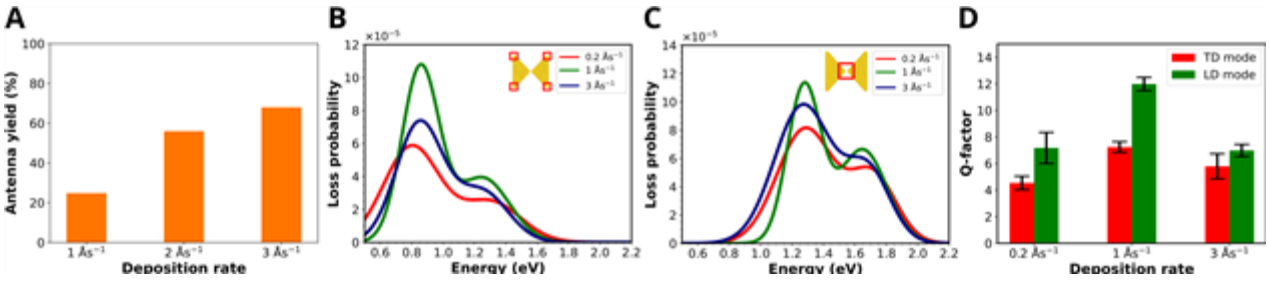

Keywords:

gold films; plasmonic antennas; EELS

Reference:

[1] M. Horák et al., Scientific Reports 8 (2018), p. 9640.
[2] L. Kejík et al., Opt. Express 28 (2020), p. 34960-34972.
[3] M. Horák, T. Šikola, Ultramicroscopy 2016 (2020), p. 113044.
[4] M. Foltýn et al., submitted (2024).

915

Analysis of photon bunching in coherent cathodoluminescence

Mr Sotatsu Yanagimoto[1], Dr Naoki Yamamoto[1], Dr Takumi Sannomiya[1], Dr Keiichirou Akiba[1,2]
[1]Tokyo Institute of Technology, Nagatsuta, Midoriku, Yokohama,, Japan, [2]National Institutes for Quantum Science and Technology, Watanuki, Takasaki, Japan

Poster Group 2

Background
Cathodoluminescence (CL) microscopy, utilizing an electron beam of an electron microscope, is a powerful approach for accessing nanoscale optical information of materials and devices. Furthermore, the time correlation measurement of CL by the Hanbury-Brown=Twiss (HBT) interferometer enables lifetime analysis without pulsing the electron beam by utilizing the photon bunching features [1]. This CL-HBT microscopy has been applied in various ways, such as lifetime measurements of semiconductors and dielectrics [2] and evaluations of the Purcell effect [3]. The origin of the bunching in CL has been investigated through a semiclassical description [4] and descriptions starting from quantum master equation [5] and is understood to be due to the random time modulation of excitation event by the fast electrons. The CL process can be classified into two classes depending on their excitation mechanisms, namely coherent CL (CCL) and incoherent CL (ICL). In the CCL process, fast electrons directly generate photons, e.g., transition radiation or Cherenkov radiation. On the other hand, in the ICL, photons are indirectly excited through mediator particles, such as bulk plasmons or secondary electrons, thus involving relaxation processes. Examples of the ICL are emission from defects and semiconductors. It is theoretically expected that the photon bunching can be observed even in CCL as far as emission events of two or more photons are included. However, most discussions on photon bunching using CL-HBT focused on ICL, and few studies have been reported regarding CCL. In this study, we experimentally confirmed the bunching phenomenon in CCL. By formulating the correlation function, we propose a method to extract the photon statistics in individual excitation events, excluding the bunching enhancement effect due to the excitation timing modulation.
Methods
Considering the semiclassical model, where n-photons are excited by a single electron, split by a half-beam splitter, and then detected by two single-photon detectors, the correlation function can be formulated. The analytical formula includes the parameters of electron beam current, correlation time and inherent correlation factor which reflects the fluctuation of the number of photons excited by a single electron. In CCL, it is expected that the photon statistics follow the Poisson distribution, and the inherent correlation factor should equal to unity. We performed this statistical analysis for localized surface plasmon (LSP) radiation, which is one of the typical examples of CCL, using a silver nanosphere with a diameter of approximately 200 nm, as schematically shown in Fig.1 (a).
We utilized a scanning transmission electron microscope (STEM) equipped with a CL detection unit and an HBT interferometer [3]. The light emitted from the sample was guided out of the STEM column by a parabolic mirror to the HBT measurement system. We performed the measurement at room temperature at an accelerating voltage of 160 kV.
Results
From the HBT measurement of the LSP radiation, we observed photon bunching, as shown in Fig. 1(b). The correlation time is approximately 400 ps, which reflects only the temporal resolution of our instrument, indicating that the lifetime of LSP is extremely short and cannot be resolved. We can observe a trend where the bunching height decreases with an increase in the electron beam current. Figure 1(c) shows an inversely proportional dependence of the correlation function on the electron beam current; such a tendency is described from our analytical formula. On the other hand, from Fig.1 (d), the values of the inherent correlation factors are approximately 1 for all the beam currents.

This suggests that the photon statistics of LSP radiation follow the Poisson distribution, which is consistent with the theoretical predictions. Additionally, the independence of the inherent correlation factor on the electron beam current indicates that the pure photon statistics by a single electron excitation is effectively extracted by removing the effect of the time modulation of the excitation event by fast electrons.

Conclusions

Through the analysis of the correlation function obtained from the HBT measurement of CL, we successfully extracted the coefficient which reflects the fluctuation of the number of photons excited by a single electron. We believe that this method is useful to investigate the elementary processes of photon generation by fast electrons.

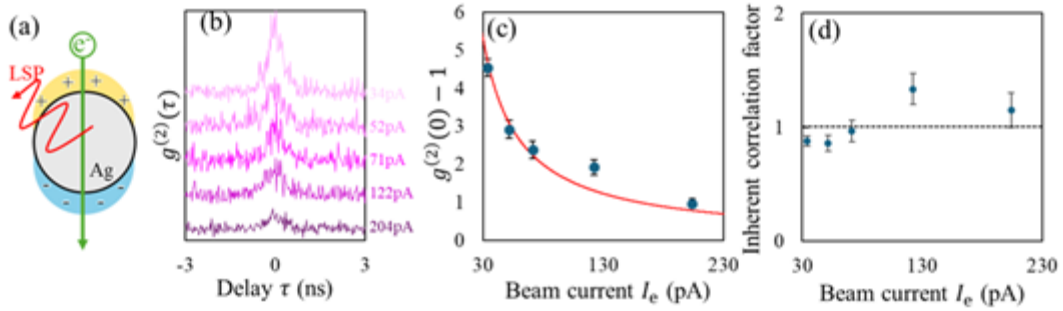

Fig.1 (a) Diagram of the LSP radiation from silver nano-sphere. (b) Correlation curves obtained with the varying electron beam current. (c), (d) Electron beam current dependency of the correlation function and the inherent correlation factor, respectively. The red solid line in (c) indicates the fitting curve with the function of inverse proportion.

Keywords:

Cathodoluminescence, Photon statistics

Reference:

[1] S. Meuret, et.al., Photon Bunching in Cathodoluminescence, Phys Rev Lett 114, (2015).

[2] S. Meuret, et.al., Lifetime Measurements Well below the Optical Diffraction Limit, ACS Photonics 3, 1157 (2016).

[3] S. Yanagimoto, et.al., Purcell Effect of Nitrogen-Vacancy Centers in Nanodiamond Coupled to Propagating and Localized Surface Plasmons Revealed by Photon-Correlation Cathodoluminescence, Phys Rev B 103, 205418 (2021).

[4] M. Sola-Garcia, et.al., Photon Statistics of Incoherent Cathodoluminescence with Continuous and Pulsed Electron Beams, ACS Photonics 8, 916 (2021).

[5] T. Yuge, et.al., PHYSICAL REVIEW B 107 , 165303 (2023) Superbunching in Cathodoluminescence : A Master Equation Approach, Phys Rev B 107, 165303 (2023).

945

Resonant inelastic light scattering micro-spectroscopy to probe inter-moiré miniband excitations in twisted 2D semiconductors

Dr. Nihit Saigal[1,2], Dr. Lennart Klebl[3], Mr. Hendrik Lambers[1], Mr. Sina Bahmanyar[1], Mr. Veljko Antić[1], Prof. Dante Kennes[4,5], Prof. Tim Wehling[3,6], Prof. Ursula Wurstbauer[1,7]
[1]Institute of Physics, University of Münster, Wilhelm-Klemm-Str. 10, 48149 Münster, Germany, Münster, Germany, [2]EMBL Imaging Center, European Molecular Biology Laboratory, Meyerhofstr. 1, 69117 Heidelberg, Germany, Heidelberg, Germany, [3]Institute of Theoretical Physics, University of Hamburg, Notkestrasse 9, 22607 Hamburg, Germany, Hamburg, Germany, [4]Institute for Theory of Statistical Physics, RWTH Aachen University, and JARA Fundamentals of Future Information Technology, 52062 Aachen, Germany, Aachen, Germany, [5]Max Planck Institute for the Structure and Dynamics of Matter, Center for Free Electron Laser Science, 22761 Hamburg, Germany, Hamburg, Germany, [6]The Hamburg Centre for Ultrafast Imaging, 22761 Hamburg, Germany, Hamburg, Germany, [7]Center for Soft Nanoscience (SoN), Busso-Peus-Str. 10, 48149 Münster, Germany, Münster, Germany

Poster Group 2

Background incl. aims:
Resonant inelastic light scattering (RILS) is a powerful technique to study collective charge excitations in semiconductor quantum nanostructures including quantum wells and nanowires [1]. The application of this technique to probe collective behavior of electrons and holes in novel two-dimensional (2D) materials has not been explored yet. The moiré superlattice potential in twisted 2D semiconductors, e.g. WSe_2, leads to carrier localization and emergence of (flat) moiré bands in the electronic band structure, which host interesting correlation physics [2]. Although the signatures of such flat bands have been shown in recent studies including scanning tunneling spectroscopy (STS) [3] and angle resolved photoemission spectroscopy (ARPES) [4] , the observation of electronic transitions between them proving the emergence of these bands, especially near the K-point of the electronic structure, have remained elusive. In this work, we used RILS micro-spectroscopy to probe the inter-moiré band excitations (IMBE) in twisted bilayers of WSe_2 with a twist angle of ~3° and ~8°.

Methods:
The twisted WSe_2 bilayers were mechanically exfoliated from bulk crystals of WSe_2 using a dry deterministic transfer technique based on viscoelastic stamps. The bilayers were also encapsulated in multilayers of hBN to protect them from environment and to provide atomically flat interfaces. The multilayer stack was built upon a ~300nm silicon dioxide layer thermally grown on p-doped silicon substrate. After preparation, the samples were annealed in vacuum and then mounted inside a refrigerator and cooled down to 4K using liquid Helium. Different regions of the sample were identified using a white LED source and Köhler illumination in combination with piezoelectric x-y-z stages and imaged using a CMOS camera. The twisted bilayer regions of the sample were optically excited using a laser beam from a frequency tunable Ti : Sa laser (linewidth = 50 KHz), cleaned up using a monochromator (1nm bandpass) and coupled to the sample through a large numerical aperture (NA = 0.82) objective lens which is compatible with low temperatures. The excitation energies were chosen near the direct optical bandgap at the K-point pre-determined using photoluminescence spectroscopy. The laser spot size on the sample was ~2µm. The emitted and scattered light from the sample was collected using the same objective and guided to a triple-spectrometer operated in a subtractive mode to reject any stray light. The RILS spectra were recorded using a liquid nitrogen cooled CCD camera.

Results:
Our results show the signatures of transitions between the 1st and 2nd moiré bands for the twist angle of ~8° and between the 1st moiré band and 2nd, 3rd and higher moiré bands for a twist of ~3° [5] We further compare our results with the RILS spectra of natural bilayers of WSe_2 where the absence of IMBE as a consequence of absence of a moiré superlattice further consolidates our results. The IMBE transition energies are in excellent agreement with those expected from theoretical ab-initio calculations in spite of broadening resulting from twist angle disorder and non-vertical transitions [5].

Conclusions:
Our results quantify the IMBE energies at the K-point of the electronic structure, where the states relevant for correlation physics are hosted. They further establish low temperature RILS as a powerful non-invasive technique for probing collective charge excitations in twisted 2D semiconductors [5].

Keywords:

2D materials, RILS, moiré minibands

Reference:

[1] A. Pinczuk et. al, Phys. Rev. Lett. 27, 317 (1971).
[2] F. Wu et. al, Phys. Rev. Lett. 121, 026402 (2018).
[3] Z. Zhang et. al, Nature Physics 16, 1093 (2020).
[4] G. Gatti et. al, Phys. Rev. Lett. 131, 046401 (2023).
[5] N. Saigal et. al, arXiv:2310.14417v1 (2023).The authors acknowledge DFG for support via Grants WU 637/7-1, WE 5342/5-1 and the SPP 2244 “2DMP” - 443273985, 443274199 and computing time granted through JARA on JURECA at Forschungszentrum Jülich. LK acknowledges support from the DFG through FOR 5249 (QUAST, P. No. 449872909). TW acknowledges support by the Cluster of Excellence ‘CUI: Advanced Imaging of Matter’ of the DFG (EXC 2056, P. ID 390715994). DMK acknowledges support by the DFG, under Cluster of Excellence Matter and Light for Quantum Computing (ML4Q) EXC 2004/1 - 390534769. We acknowledge support by the Max Planck-New York City Center for Nonequilibrium Quantum Phenomena.

953

Study of nanolaser optical and structural properties at the nanometer scale

PhD Student Cléo Santini[1], Nika van Nielen[2], Pierre-Marie Coulon[3], Stéphane Vézian[3], Julien Brault[3], Philip A. Shields[5], Albert Polman[2], Benjamin Damilano[3], Christelle Brimont[4], Thierry Guillet[4], Sophie Meuret[1]
[1]CEMES, Toulouse, France, [2]AMOLF, Amsterdam, Netherlands, [3]CRHEA, Valbonne, France, [4]L2C, Montpellier, France, [5]University of Bath, , United Kingdom

Poster Group 2

Background incl. aims
Since their first demonstration by Huang et al in 2001[1], semiconductor nanolasers have attracted a lot of interest especially for their application in optoelectronic devices. They have the advantages to be cost-effective, easy to fabricate and of a micron size. Since 2001, various semiconductors and geometries demonstrated lasing properties, for example ZnO[1] or GaN [2] nanowires act as nanolasers.
Lasing could be induced by optical pumping, usually it is characterized by a drastic reduction of the emission spectrum width, increase of the light coherence evidenced by interferences of laser diffracted light. The most significant lasing properties of nanolasers are the value of the lasing threshold, the emission wavelength (see Figure 1) and the reduction of the carrier lifetime. Moreover, nanolasers emission wavelength above the lasing threshold are linked to the laser cavity's resonance modes, which in our case is the nanowire itself. Thus, the shape of the nanowire and the laser characteristics are closely related. Due the nanoscale variation, electron microscopy is a suitable technique to examine its nanoscopic characteristics. Therefore, it is essential to link the lasing properties with the nanolaser shape and the local luminescence.
Methods
We particularly focused on the use of cathodoluminescence in a scanning electron microscope (SEM) and a scanning transmission electron microscope (STEM) to characterize the optical properties of GaN nanowires. In both microscopes, the focalised electron beam locally creates charge carriers in the semiconductor, in a pear of interaction of either hundreds of nanometers (SEM) or tens of nanometers (STEM). We studied the luminescence due to carriers recombination. Using a spectrometer, we can obtain a spectrally resolved map of the sample emission. In time-resolved electron microscopy, we are able to measure the charge carrier lifetime thank to the decay curve of the luminescence after an electron pulse (30 ps in SEM and 300 fs in STEM). . In this project we measure the lasing threshold and the cavity mode of single nanolasers and correlate the results to their nanoscale geometry and optical properties using cathodoluminescence and time-resolved cathodoluminescence measured both in STEM and SEM.
Results
We investigated the lasing properties using micro-photoluminescence UV[4] of several nanolasers and observed strong heterogeneity in the lasing mode and lasing threshold. As expected, we found that the side-pumped nanolaser had a lower energy threshold than the vertically pumped ones[5], and we observe strong variation with the nanolaser radius. We observe the same nanolaser in cathodoluminescence and obtain spectrally and spatially resolved intensity maps, that show strong intensity and spectral variation along the nanowire. Moreover, time-resolved cathodoluminescence showed that the CL decay time varies from 90 ps to 130 ps when the nanolaser radius varies from 200nm to 500nm.
Conclusion
Finally, one of the main actual challenge on the nanolaser is to link the nano-laser shape to the lasing luminescence. In this project, we combine electron microscopy to study the cavity properties with

both photoluminescence and cathodoluminescence, permitting to study respectively the macroscopic and microscopic luminescence properties.

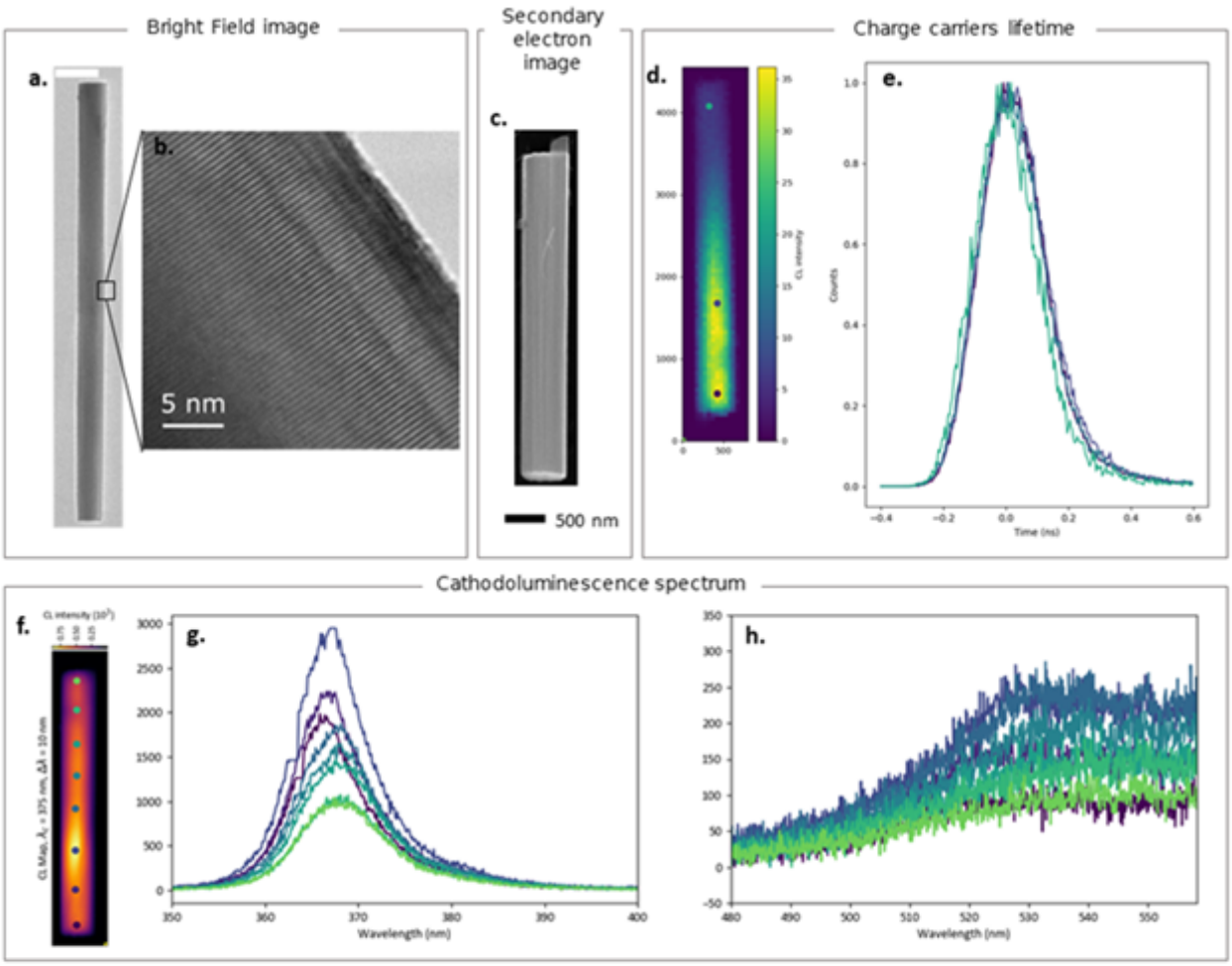

Figure 1: a.b. TEM bright field image of a nanolaser c. SEM Secondary electron image of the nanolaser studied in cathodoluminescence in d-h d. Nanolaser intensity map extracted from the time resolved cathodoluminescence dataset e. Time-resolved cathodoluminescence decay trace at different points of the nanolaser (shown in d) f. Cathodoluminescence intensity map of the nanolaser at 368nm with a bandwidth of 10nm g,h. Cathodoluminescence spectra at different positions on the nanolaser (shown in f)

Keywords:

Nanolasers
Time-resolved_Cathodoluminescence
Photoluminescence
Cathodoluminescence
III-N_Semiconductors

Reference:

[1] M. H. Huang et al., “Room-Temperature Ultraviolet Nanowire Nanolasers,” Science, vol. 292, no. 5523, pp. 1897–1899, Jun. 2001, doi: 10.1126/science.1060367.
[2] J. C. Johnson, H.-J. Choi, K. P. Knutsen, R. D. Schaller, P. Yang, and R. J. Saykally, “Single gallium nitride nanowire lasers,” Nat. Mater., vol. 1, no. 2, pp. 106–110, Oct. 2002, doi: 10.1038/nmat728.
[3] J. Binder et al., “Dynamics of thermalization in GaInN/GaN quantum wells grown on ammonothermal GaN,” J. Appl. Phys., vol. 114, no. 22, p. 223504, Dec. 2013, doi: 10.1063/1.4845715.
[4] J. Sellés, G. Cassabois, and T. Guillet, “Optical spectroscopy of GaN/AlN nanostructures embedded in planar microcavities and microdisks,” Université de Montpellier, 2015.

[5] J. Li et al., “Wavelength Tunable CdSe Nanowire Lasers Based on the Absorption-Emission-Absorption Process,” Adv. Mater., vol. 25, no. 6, pp. 833–837, Feb. 2013, doi: 10.1002/adma.201203692.

957

Improved conventional TEM sample preparation exploiting the birefringence of materials

Aleksander Brozyniak[1], Karin Stadlmann[1], Philipp Kürnsteiner[1], Heiko Groiss[1]
[1]Christian Doppler Laboratory for Nanoscale Phase Transformations, Center for Surface and Nanoanalytics, Johannes Kepler University Linz, Linz, Austria

Poster Group 2

Background incl. aims
Specimens for quality transmission electron microscopy (TEM) analyses must fulfil a range of requirements, which demand high precision during the prior preparation process. The exploitation of thickness-dependent interference colors occurring in birefringent materials can be used for an optimized procedure for conventional TEM specimen preparation. Birefringent materials display thickness-dependent interference colors in transmitted polarized light, which is analyzed by a second polarizer. The polarized light passing through a birefringent crystal splits into two components based on the refractive indices, resulting in an optical path difference called retardation. Recombining both components with the analyzer leads to annihilation of specific wavelengths through destructive interference, revealing observable interference colors. This phenomenon was first described by Auguste Michel-Lévy at the end of the 19th century along with a color chart of perpendicularly aligned polarizers for various birefringence values.
Methods
Our study leverages this phenomenon to optimize mechanical thinning in conventional sample preparation for transmission electron microscopy (TEM) [1]. For our experiments we employ two prominent semiconductor substrate materials from industry and research exhibiting birefringence: silicon carbide (4H-SiC) and sapphire (Al_2O_3). Figure 1 (a) displays the section of the Michel-Lévy chart containing the orange dotted 0.008-birefringence line of Al_2O_3 and the cyan dotted 0.056-birefringence line of 4H-SiC. We discuss our findings on dimpled and wedge-polished two-materials specimens, which are composed from a two-layer stack combining 4H-SiC and Al_2O_3 in one specimen. Top-view polarization microscopy images of the dimpled Al_2O_3/4H-SiC sample and the wedge-polished Al_2O_3/4H-SiC sample can be seen in Figure 1 (b) and 1 (c), respectively. For materials with small birefringence like Al_2O_3, where interference colors vanish at smaller thicknesses, we propose a complementary color chart for a parallel polarizer orientation, supplementing the Michel-Lévy chart for crossed polarizers.
Results
The thickness of the thinnest sample region can be estimated visually, with its color directly corresponding to the thickness on a color chart. During thinning, simple geometrical models that assume the specimen shape in dimple and wedge geometry can help to determine the thickness at the thinnest specimen position. A more complex RGB analysis of the occurring colors allows for measuring the required lateral fringes position with high accuracy. In all cases the achieved accuracy of thickness monitoring, validated by scanning electron microscopy (SEM), significantly exceeds the measurement capabilities of built-in mechanical gauges in thinning instruments.
Conclusion
Our proposed method facilitates a highly accurate determination of specimen thickness to avoid damage or breaking during mechanical thinning and reduces ion-milling times. The benefits of the approach are shown on sapphire and silicon carbide cross-section samples. The presented method is equally suitable for assessing specimen thickness during dimpling and wedge-polishing, and is particularly useful at thicknesses below 20 µm, where the accuracy of mechanical techniques is insufficient. It is precise enough to be employed for a visual thickness estimation during the thinning process, but can be additionally optimized by analyzing the RGB spectrum of the occurring

interference colors. It is applicable to all materials if additional birefringent materials serve as a thickness reference during polishing.

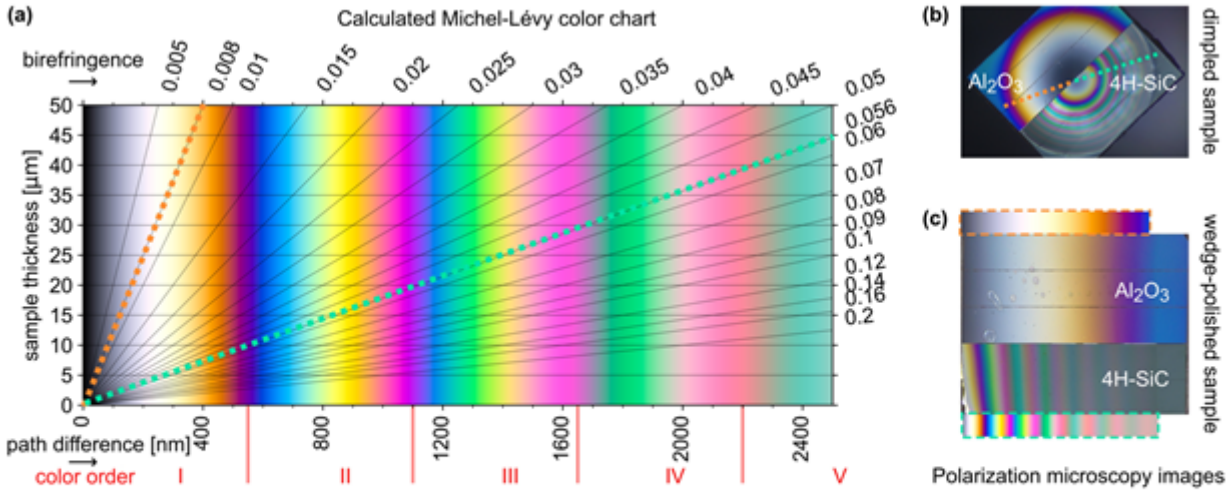

Figure 1 (a) Section of the Michel-Lévy chart containing the orange dotted 0.008-birefringence line of Al_2O_3 and the cyan dotted 0.056-birefringence line of 4H-SiC.; Top-view polarization microscopy image of **(b)** the dimpled Al_2O_3/4H-SiC sample and **(c)** the wedge-polished Al_2O_3/4H-SiC sample, with attached respective sections of the Michel-Lévy chart in orange and cyan dashed line frames.

Keywords:

Preparation, Birefringence, Dimpling, Wedge Polishing

Reference:

A. Brozyniak, K. Stadlmann, P. Kürnsteiner, H. Groiss, Micron 177 (2024) 103580

1003

Investigating the photoelectronic properties of MoS2 thin layer with ITO nanoparticles using photoluminescence and cathodoluminescence

Mr Andrea Cicconardi[1,2], Dr Andrea Griesi[1], Dr Gunnar Kusch[4], Dr Silvia Dante[1], Prof Rachel Oliver[4], Dr Ilka Kriegel[1,3], Dr Giorgio Divitini[1]
[1]Istituto Italiano di Tecnologia, Genova, Italy, [2]University of Genova, Genova, Italy, [3]Istituto Italiano di Tecnologia, Turino, Italy, [4]University of Cambridge, Cambridge, United Kingdom

Poster Group 2

Background
The development of sustainable, renewable energy requires novel solutions that enabling energy storage and conversion, for example for smoothing unstable/variable energy sources.
In order to do so, we can design nanostructures that can trap charge, utilising metal oxide (MO), such as Sn-doped In2O3 nanocrystals (ITO NCs). In ITO, aliovalent substitutional doping can effectively modulate charge carrier density. (1) The bandgap for ITO NCs, crucial for band engineering, is between 3.5 eV and 4.3 eV. (2) (3)
Molybdenum disulphide (MoS2) is a transition metal dichalcogenide (TMDC) semiconductor with an indirect bandgap of 1.3 eV in bulk form, while a direct bandgap of 1.8 eV when in a monolayer. (4)
In this work we use a combination of optical and electron spectroscopy to locally analyse the photodoping phenomenon, a light-driven charge accumulation of electrons, on ITO NCs when coupled with MoS2 monolayer, that act as a sacrificial hole scavenger, deposited on a SiO2 substrate. The innovation of this device lies in the dual role of converting solar energy and storing the resulting charges.

Methods
Photoluminescence (PL) denotes the emission of light from a material after the absorption of photons (electromagnetic radiation). The light emission occurs following photoexcitation, wherein incident photons promote electrons to higher energy states. The Micro-PL was measured using an inVia Renishaw Raman microscope with an excitation laser at 488nm.
Cathodoluminescence (CL) is an optical and electromagnetic phenomenon wherein electrons, typically in a scanning electron microscope, induce the emission of photons, often characterised by wavelengths within the visible spectrum.
CL data were acquired in an Attolight Allalin 4027 Chronos SEM-CL. The spectra were acquired with an iHR320 spectrometer) and an Andor 1024 pixel charge-coupled device. All the measurements were performed at room temperature under high vacuum (<10−7 10 80 100 mbar) with an acceleration voltage of 3 kv. Data were analysed using Lumispy / Hyperspy.

Results
By studying local PL and CL in correlation to the presence of specific MoS2 morphologies, such as monolayer, folded layers and other localised alterations, particularly in the vicinity of the ITO NCs, we aim to understand the local charge dynamics and the interplay between the MoS2 and the NCs.
Our observations reveal a notable reduction in emission intensity in areas surrounding and within the ITO-rich region, which we ascribe to successful charge transfer. The extent of the process is studied in 2D, and results from PL and CL are compared, providing information on different lengthscales and response to different excitation intensities.

Conclusion
Devices incorporating Indium Tin Oxide (ITO) nanocrystals (NCs) and MoS2, where photodoping occurs, present promising solutions for direct solar-to-charge conversion and storage. The parallel

use of cathodoluminescence (CL) and photoluminescence (PL) enables a comprehensive evaluation of these properties at sub-micron lateral resolution.

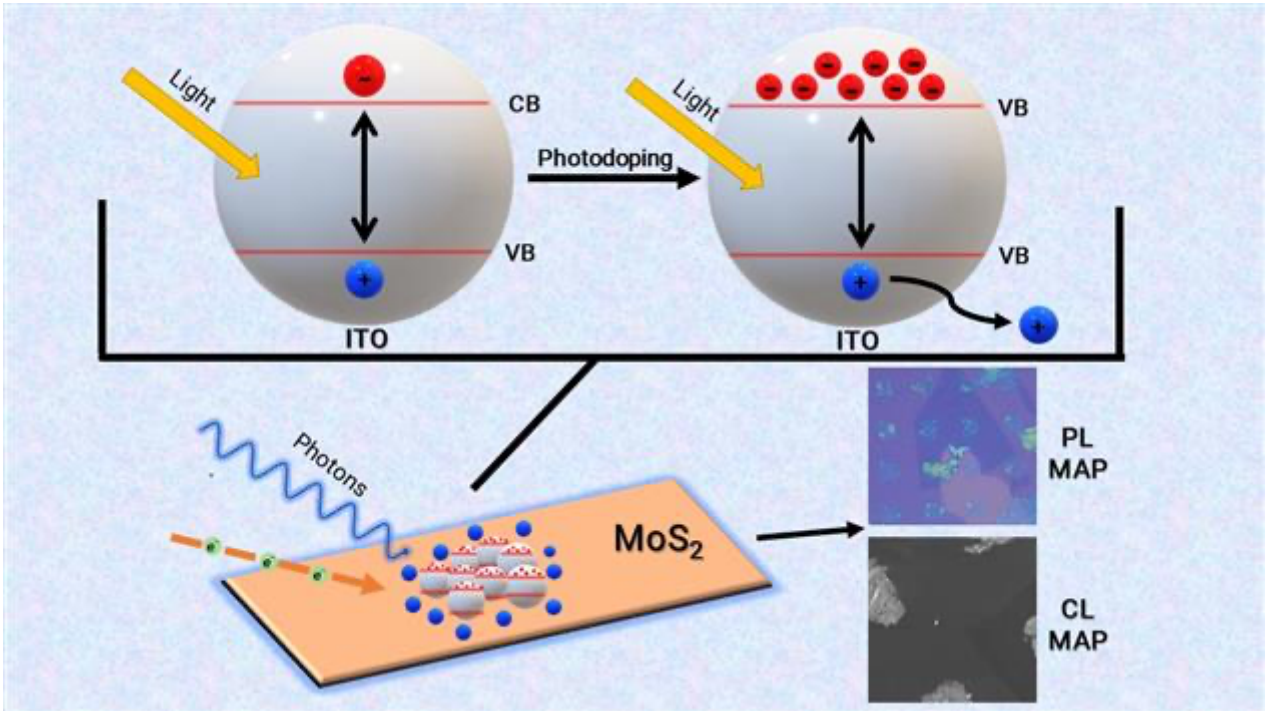

Keywords:

Photodoping, Photoluminescence, Cathodoluminescence, ITO, MoS2

Reference:

1. Michele Ghini, Andrea Rubino, Andrea Camellini, and Ilka Kriegel. Multi-charge transfer from photodoped ITO nanocrystals. Nanoscale Adv. 3, 2021, Vol. 23.

2. Yu, Z., Perera, I., Daeneke, T. et al. Indium tin oxide as a semiconductor material in efficient p-type dye-sensitized solar cells. NPG Asia Mater. 305, 2016, Vol. 8.

3. I. Hamberg, C. G. Granqvist, K. -F. Berggren, B. E. Sernelius, and L. Engström. Band-gap widening in heavily Sn-doped In2O3. Physical Review B. 1984, Vol. 30.

4. Wang, Qing Hua & Kalantar-zadeh, Kourosh & Kis, Andras & Coleman, Jonathan & Strano, Michael. Electronics and Optoelectronics of Two-Dimensional Transition Metal Dichalcogenides. Nature nanotechnology. 2012, Vol. 7, pp. 699-712.

1024

Structural and Compositional Investigation of Ag-Incorporated CsPbBr3 Nanocrystal Heterostructures

Dr Sirous Khabbaz Abkenar[1], Ms. Anna Cabona[2,3], Mr. Basem Ameen Ahmed Qahtan[1,3], Dr. Stefano Toso[2], Dr. Andrea Griesi[1], Prof. Liberato Manna[2], Dr. Giorgio Divitini[1]
[1] Istituto Italiano di Tecnologia, Electron Spectroscopy and Nanoscopy, Genova, Italy, [2]Istituto Italiano di Tecnologia, Nanochemistry, Genova, Italy, [3]Dipartimento di Chimica e Chimica Industriale, Università degli Studi di Genova, Genova, Italy

Poster Group 2

Background
The fabrication of halide perovskite-based heterostructures represents a promising avenue in the field of optoelectronics due to their unique properties arising from the heterointerface between a perovskite domain and a domain of another material [1]. When CsPbBr3 is interfaced with a compound with a different band gap, the heterointerface acts as a barrier for charge carriers, affecting their transport properties and recombination dynamics, which consequently leads to significant changes in electronic structure [1, 2]. Such tunable optical and electronic properties, together with increased structural rigidity introduced into the perovskite lattice, allow for the development of novel optoelectronics with improved performance and functionality compared to the standalone CsPbBr3-based devices. Nano-scale understanding of the structural and compositional characteristics of such heterostructures within the two domains as well as across the interface plays a pivotal role in the design and engineering of advanced optoelectronic devices. Herein, we conduct a study to characterize the structural features in CsPbBr3/AgBr heterostructures obtained via a colloidal synthesis method [3] by using advanced electron microscopy techniques at the nanoscale.
By combining HRSTEM, hyperspectral imaging, and harnessing advanced data treatment approaches, we sought to explore the structure, morphology, and subtle compositional changes at the heterointerface as well as the crystal domains of such beam-sensitive materials for optimization of optoelectronic performance.

Methods
The heterostructures were prepared for TEM analysis by dispersing the powders in hexane and then drop-casting them onto Cu grids with a carbon support film. Preliminary investigations of the nanocrystals were carried out using an image-Cs-corrected JEOL JEM-2200FS with a Schottky emitter gun operated at 200 kV, equipped with a Bruker XFlash5060 silicon-drift detector (SDD) for energy-dispersive X-ray spectroscopy.
To visualise the crystal lattice of the heterostructure domains, scanning transmission electron microscopy (STEM) images were acquired using Annular Bright Field (ABF) and High-Angle Annular Dark Field (HAADF) detectors on a probe-aberration-corrected ThermoFisher Spectra 300 S/TEM microscope with an X-FEG source, operated at 300 kV. For precise structural imaging, a drift correction frame integration technique in Velox was used to minimize image distortions. Elemental distribution maps and line scan profiles at high spatial resolution were recorded by collecting Energy-Dispersive X-ray (EDX) signals on a Dual-X system, which comprises two EDX detectors positioned on either side of the specimen, with a total collection solid angle of ca. 1.76 sr, allowing for efficient signal acquisition from nanocrystals.
Furthermore, we combined a machine learning-based segmentation algorithm with hyperspectral EDX datasets to obtain a comprehensive statistical understanding of the chemical composition of the nanocrystals.

Results

STEM-HAADF images showed different possible morphologies for the nanocrystal heterostructures. We identified well-defined heterostructures with a sharp heterointerface in lateral projection, composed of 2 structural domains. EDX elemental maps revealed that Ag was localized in the higher contrast domains correlating with a uniform distribution of Br, which was consistent with the retention of AgBr composition in such domains. The lower contrast domains contained predominantly signals from Cs, Pb, and Br, corresponding to the CsPbBr3 according to the quantification of the compositional EDX spectra. In these heterostructures, we also noted the segregation of metallic Ag within the structural features, which we ascribed to local electron beam damage.

In addition to intact cubes of CsPbBr3 nanocrystals, CsPbBr3/metallic Ag as well as non-stoichiometric silver bromide nanostructures, compositional maps additionally showed the formation of potential heterostructures with a spherical morphology in which Ag was mainly localized at the nanocrystal edges, producing a core-shell structure. We also characterized nanocrystals preserving the superimposition of AgBr and CsPbBr3 stoichiometries without a clearly defined interface. However, differentiation of such potential heterostructures from other nanocrystals in this nanosystem is difficult due to similarity in elemental composition, resulting in insufficient contrast in HAADF images. While the analysis of individual particles by hand is often inconclusive, we apply machine learning-based routines to segment nanoparticles in hyperspectral images on large fields of view, followed by quantification of composition for each, enabling us to obtain operator-agnostic statistical insight into the composition of nanocrystals in this complex system.

Furthermore, by combining ABF and HAADF imaging, we were able to visualise atomic columns of light and heavy elements in CsPbBr3/AgBr lateral heterostructures simultaneously, providing crucial details about the crystal lattice structure and the interface.

Conclusion

Through the combined use of electron microscopy techniques, including imaging and spectroscopy, we achieved a comprehensive understanding of the structural and compositional characteristics of heterostructures formed via the incorporation of Ag-precursor during colloidal synthesis of lead halide perovskites – in particular CsPbBr3 – at nanoscale resolution. This spatially-resolved structural information, together with high-throughput analysis of compositional hyperspectral EDX datasets using machine learning-assisted methods, contributes to the efficient interpretation of unique optical properties such as tunable band gap, new charge carrier transmission modes, and high photoluminescence quantum efficiency in such materials for application in high-performing optoelectronic perovskite devices.

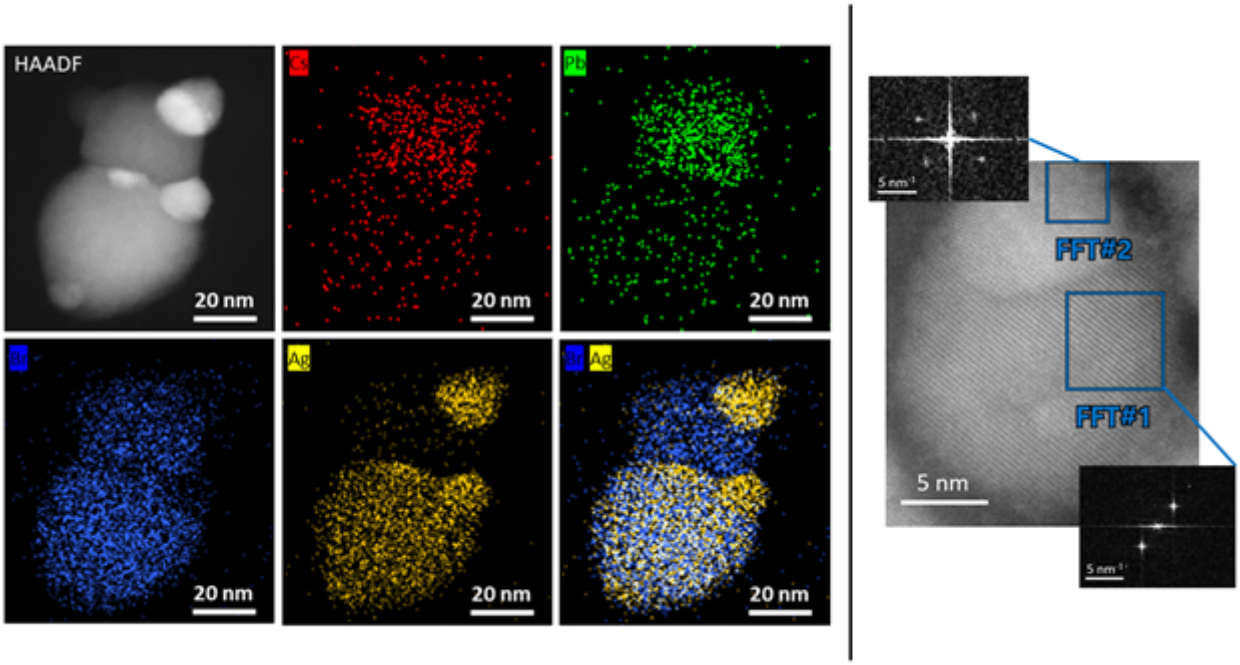

Keywords:

Hyperspectral Mapping, Perovskites, Heterostructure, Heterointerface

Reference:

1. Cheng, X., Y. Han, and B.B. Cui, Fabrication Strategies and Optoelectronic Applications of Perovskite Heterostructures. Advanced Optical Materials, 2021. 10(5).
2. Imran, M., et al., Halide Perovskite-Lead Chalcohalide Nanocrystal Heterostructures. J Am Chem Soc, 2021. 143(3): p. 1435-1446.
3. Rusch, P., et al., Nanocrystal Heterostructures Based On Halide Perovskites and Lead–Bismuth Chalcogenides. Chemistry of Materials, 2023. 35(24): p. 10684-10693.

1091

Microstructure of light-emitting phosphor of (Sr, Ca)AlSiN3:Eu2+

Hajime Matsumoto[1]
[1]Mitsubishi Chemical Corp., Yokohama, Japan, [2]National Institute for Materials Science, Tsukuba, Japan

Poster Group 2

If the peak half-maximum width of the emission spectrum is wide, the emission of light at wavelengths far from the target emission peak wavelength may increase, and the emission color indicating the desired chromaticity coordinates may not be obtained. In addition, in the case of red phosphors, the emission of light increases in wavelength regions with low specific visual sensitivity, such as 700 nm or more, which contributes to a decrease in the conversion efficiency of the light-emitting device. For this reason, phosphors with a narrower peak half-maximum width are required.

(Sr, Ca) AlSiN3:Eu2+ (SCASN) is a red phosphor [1] with a narrower peak half-width in the emission spectrum than CaAlSiN3:Eu2+ (CASN). These phosphors are highly reliable because they replace the Al site of AlN with Sr, Ca, and Si. In this study, we present the first microscopic results obtained for this type of materials.

SCASN and CASN have the same crystal structure, space group: Cmc21, which was investigated by the convergent beam electron diffraction (CBED) technique and the integrated differential phase contrast STEM (iDPC-STEM) technique. In the case of SCASN, the structure of the spatial group: Pcbn was also confirmed in the selected area of diffraction pattern, which was found to be due to the local atomic arrangement of the stacking fault. It was found using scanning moiré fringe imaging [2] that the higher the amount of Sr added in SCASN, the more dislocations and stacking fault co-exist, and that the disturbed stress distribution settles through the stacking defects in the region with high dislocation density. In addition, in SCASN manufactured by the high-pressure method, the distance between the stacking fault was far apart, and the stress distribution was stable.

These experiments have allowed the achieving of understanding of the close relationship between the ratios of Sr and Ca and the stress distribution and the extraction of significant features like the dislocation in the crystal, the stacking fault that it expanded, and the first neighbourhood distances between defects.

Keywords:

(Sr,Ca)AlSiN3, phosphor, iDPC-STEM

Reference:

[1] Kyota Uheda et al, “Luminescence properties of a red phosphor, CaAlSiN3: Eu2+ for white light emitting diodes” Electrochemical and Solid-State Letters, 9 (4), H22 (2006).

[2] Suhyun Kim et al. “Quantitative measurement of strain field in strained-channel-transistor arrays by scanning moiré fringe imaging” Appl. Phys. Lett. 103, 033523(2013).

1093

Multifunctional hybrid nanocomposite films: linking inorganic nanoparticles using α-synuclein as molecular linker

Prof Patrizia Canton[1], Prof Adolfo Speghini[2], Dr Emil Milan[2], Dr R Tira[2], Dr. M. D'Onofrio[2], Dr M Assfalg[2]
[1]Department of Molecular Sciences and Nanosystems, Ca' Foscari University of Venice , Venezia, Italy, [2]Department of Biotechnology, University of Verona, Verona, Italy

Poster Group 2

Background incl. aims
Organic-inorganic hybrid nanocomposites can combine mechanical properties and particular functionalities exploiting organic macromolecules and inorganic nanoparticles. Inorganic nanoparticles can induce peculiar properties that can be exploited in several technological fields. For instance, luminescent nanomaterials are useful in nanomedicine as contrast agents, while proteins can act as stealth agents.
Methods
The interaction of inorganic nanoparticles with proteins is a matter of particular interest when studying their behaviour in a biological environment, especially for the development of new hybrid materials. Recently, investigation on hybrid monolayers of gold nanoparticles and α-synuclein, an intrinsically disordered protein associated with some neurodegenerative diseases such as Parkinson's disease, have appeared in the literature. Due to particular variations of the chemical environment, α-synuclein undergoes structural changes from a disordered state to a β-sheet conformation that leads to the formation of fibrils, useful for the formation of hybrid films. This behavior makes α-synuclein suitable for the development of nano-biocomposite nanomaterials such as nanofilms and filaments.
Results
Hybrid films composed of inorganic nanoparticles and α-synuclein have been developed. The hybrid films have been prepared, using a wet chemistry procedure, using various types of inorganic nanoparticles, as lanthanide doped alkaline-earth fluorides, to obtain nanocomposites with strong emission in the optical range. In particular, the structure of the inorganic nanoparticles and the α-synuclein monolayer is under study by means of STEM and HREM; the nanoparticle upconversion emission, a particular process involving emission of light (e.g. in the UV-visible range) upon excitation with electromagnetic radiation of lower energy (e.g. in the Near InfraRed, NIR, range) of the nanocomposites is described. The peculiar emission of the lanthanide ions in the optical range can be very useful for applications in nanomedicine, working in the so-called biological windows, exploiting the transparency of biological tissues in certain NIR ranges. Moreover, combination of different kinds of nanoparticles (e.g. gold and luminescent fluoride based nanoparticles) have been considered to develop multifunctional films with luminescence and thermometric capability for possible applications as biosensors.

Keywords:

nano-biocomposite nanomaterials, inorganic nanoparticles, upconversion.

Reference:

J. Lee, G.Bhak, J.H. Lee, W. Park, M. Lee, D. Lee, N.L. Jeon, D. Jeong, K. Char and S.R. Paik, Angew. Chem. 2015, 54, 4571–4576.

1221

Visualization of surface plasmon propagation and emissions by cathodoluminescence

Izzah Machfuudzoh[1], Sotatsu Yanagimoto[1], Researcher Naoki Yamamoto[1], Supervisor Takumi Sannomiya[1]
[1]Tokyo Institute of Technology, Yokohama, Japan

Poster Group 1

- Background -
Plasmonic materials are capable of manipulating light-matter interactions at nanoscale dimensions through the control of material morphology. Metallic plasmonic waveguides with extended geometrical nanostructures, such as planar surfaces, periodical gratings, and nanowires, can support eigenmodes of surface plasmon polaritons (SPPs), which are defined as surface electromagnetic waves propagating along the interface between a metal and a dielectric medium. The intrinsically two-dimensional nature of SPPs provides flexibility in engineering integrated nanophotonic circuits, facilitating the transfer of optical information across given distances due to their confined and enhanced fields near the interface [1]. However, despite the importance of SPP modes in applications such as optical communications and photonics, detailed studies on their propagation and emissions upon excitation are relatively underexplored. In this work, we present an extensive study on the behavior of SPPs on one-dimensional plasmonic crystals (1D-PlCs), delving into their propagation properties as well as the simultaneous correlation of their emission positions relative to the beam irradiation spots.
- Methods -
A 1D-PlCs with a periodicity of 600 nm and terrace dimensions of 420 nm width and 100 nm height, patterned on an otherwise flat 200 nm-thick silver surface, served as the samples. Mode excitation and data acquisition were both performed in cathodoluminescence-based scanning transmission electron microscopy (STEM-CL) at an accelerating voltage of 80 kV. This modified STEM-CL system is capable of resolving the emission angles θ and energies E of the detected CL radiations, providing full post-access on the fields of the excited modes [2]. The vertically-polarized emissions from different sample setups were analyzed, namely the “flat at front” and “flat at rear” setups with half-grating-half-flat structure oriented symmetrically along the x-direction (see Figure 1).
- Results -
Distinctive dispersion curves with predominantly opposing slopes were observed. The “flat at front” setup exhibits negative-slope dispersion lines attributing to backward-propagating SPPs (in the negative x-direction), while the “flat at rear” setup with a geometrically symmetric flip shows positive-slope dispersion lines referring to forward-propagating SPPs (in the positive x-direction), as shown in Figure 1(a,b). These differences are due to the presence of periodic structures on only one side of the samples, causing the SPPs propagating towards the planar surface to experience no SPP-scattering structure. Moreover, the effect of the interference of the outcoupled SPPs as photons with transition radiation (TR) generated at the beam impact position was also clearly observed as additional dispersion lines appearing in-between, as marked by numbers in Figure 1(a,b) [3].
Photon maps analysis further elucidates the characteristics of the excited modes and spatially visualizes the interference phenomena. Two modes with distinguished hotspot distributions were observed at θ = 20°±5°: the symmetric mode (S-mode) at around E = 2.50 eV (Figure 1(d,f)) and the antisymmetric mode (A-mode) at E = 1.47 eV (Figure 1(c,e)). The former S-mode has opposite sign charges located alternatively at the terrace and groove centers, while the latter A-mode distributes the charges along the terrace edges. Additionally, periodic-like fringes with varying spacings were observed on the planar surface, depicting a spatial image of the interference of SPP-induced radiation with TR. For the A-mode, for instance, given the measured fringe spacings of 645 nm and

1190 nm respectively for the “flat at front” and “flat at rear” setups, the average SPP wavelength was estimated to be around 838 nm [4]. Such a wavelength, close to but less than its free-space wavelength of the A-mode at 843 nm, indicates the bound nature of SPPs on a flat surface.
A study on the optical emission spots was also performed to evaluate the positions of the photon emissions from the propagating SPPs upon scattering by grating structures. By synchronizing emission imaging with beam scanning on the sample, signals of the emitted CL light were captured and digitally mapped as emission spots, with each pixel in the emission space storing information about spatial emission positions in the sample space [5]. Depending on the sample setups (i.e., the “flat at front” or “flat at rear” setups) and beam excitation positions (i.e., at the terrace, groove, or flat area), the obtained emission spots varied in number (i.e., one, two, or three spots). By extracting the signals of these emission spots, known as emission-spot-decomposed CL maps, it was uncovered that photons emerge not only at where the beam is irradiated but also at more delocalized locations, providing strong evidence of the scattering of propagating SPPs. Moreover, shifts of the emission spots with beam irradiations across the samples show a nonlinear trend, depicting a modulation of the emission spots by the presence of the surface charge distributions.
- Conclusions -
In conclusion, our studies uncover how SPPs interact with 1D-PICs through their propagation behaviors, as revealed by dispersion curves with opposing slopes, CL photon maps with differing fringe widths, and optical emission spots with emission-spot-decomposed CL maps showing emission positions. This work, with in-depth details on the SPP propagation, could provide valuable insights for designing nanophotonic devices.

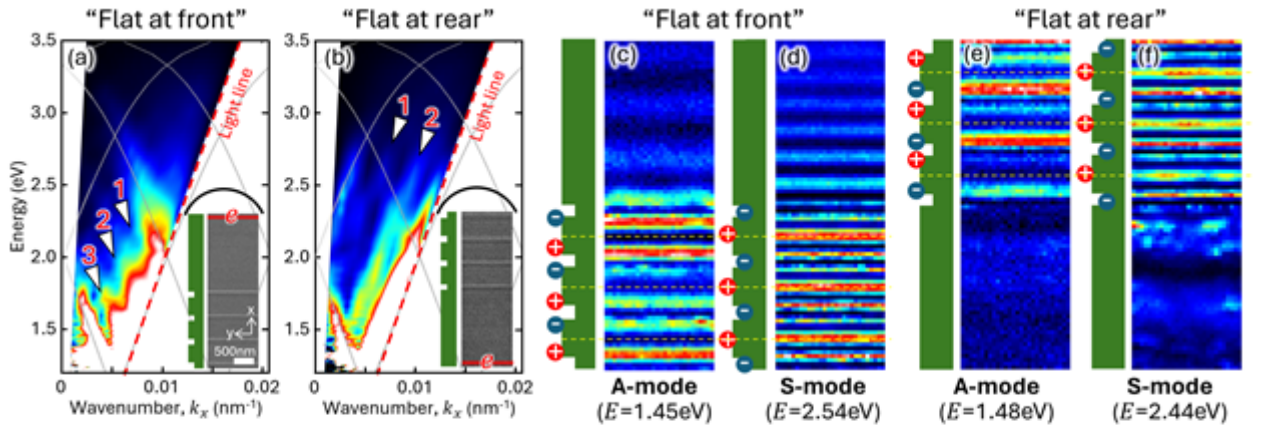

Figure 1. Area-resolved dispersion curves for the (a) “flat at front” and (b) “flat at rear” setups. Solid gray lines indicate calculated SPP dispersion curves, and the numbers mark the additional interference-induced dispersion lines. The inset shows backscattered images of the samples, with the rectangular red area representing beam excitation positions. Photon maps of the (c) A-mode and (d) S-mode for the “flat at front” setup and (e,f) the “flat at rear” setup. Charge distributions on the sample are also shown illustratively, with the dashed yellow lines indicating terrace centers.

Keywords:

Surface plasmons, transition radiation, cathodoluminescence

Reference:

[1] Fang, Y. and Sun, M., 2015. "Nanoplasmonic waveguides: towards applications in integrated nanophotonic circuits." Light: Science & Applications, 4(6), pp.e294-e294.
[2] Machfuudzoh, I., Hinamoto, T., García de Abajo, F.J., Sugimoto, H., Fujii, M. and Sannomiya, T., 2023. "Visualizing the nanoscopic field distribution of whispering-gallery modes in a dielectric sphere by cathodoluminescence." ACS Photonics, 10(5), pp.1434-1445.
[3] Sannomiya, T., Matsukata, T. and Yamamoto, N., 2024. "Controllable chiral light generation and vortex field investigation using plasmonic holes revealed by cathodoluminescence." Nano Letters, 24(3), pp.929-934.

[4] Yamamoto, N. and Suzuki, T., 2008. "Conversion of surface plasmon polaritons to light by a surface step." Applied Physics Letters, 93(9).
[5] Matsukata, T., Ogura, S., García de Abajo, F.J. and Sannomiya, T., 2022. "Simultaneous nanoscale excitation and emission mapping by cathodoluminescence." ACS Nano, 16(12), pp.21462-21470.

1316

Fabrication and charaterization of plasmonic nanopillars on a thin membrane for TEM investigation

Maria Serra González[1], Matthias Keil[1], Rucha Deshpande[1], Rafael Taboryski[1], Shima Kadkhodazadeh[1]
[1]DTU Nanolab, Kongens Lyngby, Denmark

Poster Group 1

Plasmonic resonances are characterized by a highly localized and enhanced electromagnetic field around structures the size of the excitation wave, also known as “hot-spots". This phenomenon has been exploited in recent years in fields such as sensing, imaging or catalysis. The hot-spots enhance the signal in Raman spectroscopy [1], increase sensitivity for label-free protein detection [2], or generate localized heat for catalysis [3]. In these studies, plasmonic effects are usually quantified through these secondary effects or simulations rather than the direct measurement of the electromagnetic field in the hot-spots. In this work, we present the fabrication of a plasmonic sample consisting of a nanopillar array on a thin membrane suitable for a TEM study, which will allow probing the surface plasmons (SPs) with an electron beam. Excitation of the SPs will be possible with the mounting of a white LED in the chip, and thus the electron beam will be deflected and measurable in the vicinity of the hot-spots.

For the sample fabrication, we employed a combination of resolution enhancement techniques on a DUV stepper tool namely off-axis illumination, cross- triple exposure and the addition of assist feature lines on the design [4]. We achieved a hexagonal array of nanopillars with 150 nm diameters and 350 nm pitch. Deep Reactive Ion Etching (DRIE) was employed for the silicon oxide pillars’ etch and UV lithography was used to pattern and align the openings for the membranes with an accuracy of 2 um. A KOH bath etched the back of the silicon wafer to achieve 20 nm thick membranes. Finally, a 19 nm of aluminum coating ensured the plasmonic effects. Optical characterization on a micro-spectrophotometer of the fabricated chips confirmed plasmonic resonances on the visible range, Figure 1 b). The reflectance shows a resonance dip at 500 nm wavelength that differs significantly to the reflectance in the unpatterned area of the same membrane. This proofs that the addition of nanostructures increases the absorption of light in the form of localized surface plasmons.

Additionally, the sample was mounted on a TEM grid by means of a lift-out and welding process. Using a xenon ion beam, the nanopillar membrane was released from the substrate and mounted on a TEM grid and to a TEM electrical chip welding it with tungsten, Figure 1 a). A preliminary simulation of the fabricated nanopillar presented plasmonics resonances for visible wavelengths. An example is shown in Figure 2 a) where the EM-field distribution is highly localized in the top of the pillar quadruplicating the intensity of the excitation beam of 430 nm wavelength. The spectral shape of the simulated reflectance in Figure 2 b) is a good match to the reflectance measured in Figure 1 b). The measured dip at 500 nm shifts to the simulated dip at 650 nm, still within the visible range. Thus, the model describes the physics of the structure well.

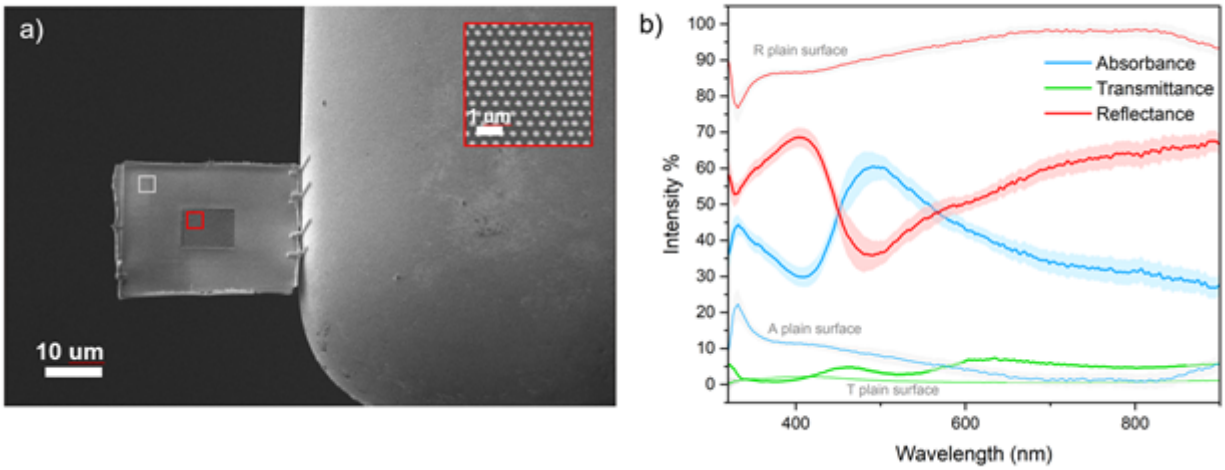

Keywords:

Plasmonic, Nanopillar, Membrane, TEM, Resonance, Reference:

[1] G. V. P. Kumar, J. Nanophotonics, 6(1),(2012), 064503
[2] P. Zhang, Nat. Methods, 17(10), (2020),1010–1017
[3] A.G.M. da Silva, ChemComm, 58(13), 82022), 2055–2074
[4] M. Serra Gonzalez, et al, J. Vac. Sci. Technol. B:Nanotechnol. Microelectron., 41(6), (2023), 063601

1215

HR STEM study of anion/cation exchange in colloidal lead halide perovskite heterostructures

Iurii Ivanov[1], Mr Nikolaos Livakas[2], Ms Juliette Zito[2], Dr. Ivan Infante[3], Prof. Liberato Manna[2], Dr. Giorgio Divitini[1]
[1]Electron Spectroscopy and Nanoscopy, Istituto Italiano di Tecnologia, , , [2]Nanochemistry, Istituto Italiano di Tecnologia, , , [3]BCMaterials, Basque Center for Materials, Applications, and Nanostructures, Ikerbasque, Basque Foundation for Science, ,

Poster Group 2

Introduction Lead halide perovskite nanocrystals (LHP NCs) with composition $CsPbX_3$ (X = Cl, Br, I) have been widely studied due to their high photoluminescence quantum yield (PLQY) and narrow emission bandwidth, covering the whole visible spectral range. These properties, together with a remarkable tolerance to surface defects, make LHP NCs quantum dots (QDs) promising candidates for various light-emitting applications. Emission tunability in such materials is typically achieved by halide alloying, produced either directly during synthesis or as a result of post-synthetic halide (anion) exchange reactions. Cl-Br and Br-I exchanges are now well understood and we have recently provided a clearer view of the $CsPbCl_3$ → $CsPbI_3$ halide exchange [1]. Another way to tune outstanding optical properties of such QDs is to bond them with other semiconductors – metal chalcogenides (MC), which also adds the possibility of employing post-synthetic cation exchange. Here we present a detailed structural and compositional study of the interfaces between LHPs and MCs and their role during post-synthetic anion/cation exchange. Methods High resolution scanning transmission electron microscopy (STEM) studies were performed in an aberration-corrected ThermoFisher Spectra 300 operated at 300 kV. Samples were prepared by drop-casting diluted solutions of NCs onto ultra-thin carbon film grids. Atomic resolution images were acquired in both HAADF and iDPC modes. Compositional maps were obtained with a Dual-X EDX detector using Velox and rapid rastered scanning of the beam. Results Figure 1 shows HR STEM HAADF images of two colloidal epitaxial LHP-MC heterostructures used as a basis for post-synthetic anion/cation exchange: $CsPbCl_3$–$Pb_4S_3Cl_2$ and $CsPbCl_3$-PbS. The Cl-I halide exchange in $CsPbCl_3$–$Pb_4S_3Cl_2$ makes it possible to stabilise two perovskite domains ($CsPbCl_3$ and $CsPbI_3$) within one colloidal NC, despite the huge difference in lattice parameters (9%). HAADF, iDPC and GPA analysis revealed a complex 3D strain distribution and key role for the LHP-MC interface during halide exchange. The newly synthesised $CsPbCl_3$-PbS epitaxial heterostructure is shown in Figure 1b,c. Based on it we could prepare, by post synthetic anion exchange, heterostructures in which the perovskite domain is either $CsPbCl_3$, $CsPbBr_3$ or alloyed $CsPb(Brx/Cl1-x)_3$. HRSTEM confirmed that anion exchange only affects the perovskite region and does not affect the PbS domain. Next, through post-synthetic cation exchange, we created heterostructures in which the MC is either PbS or Cu_2S. HR STEM and STEM-EDX data were used to construct 3D atomic models of all heteroepitaxial NCs before and after post synthetic anion/cation exchange reactions. Conclusion Using STEM, we constructed atomic models of a series of recently discovered LHP-MC heteroepitaxial colloidal QDs and linked them to the optoelectronic properties, in particular emission tunability by post synthetic anion/cation exchange reactions.

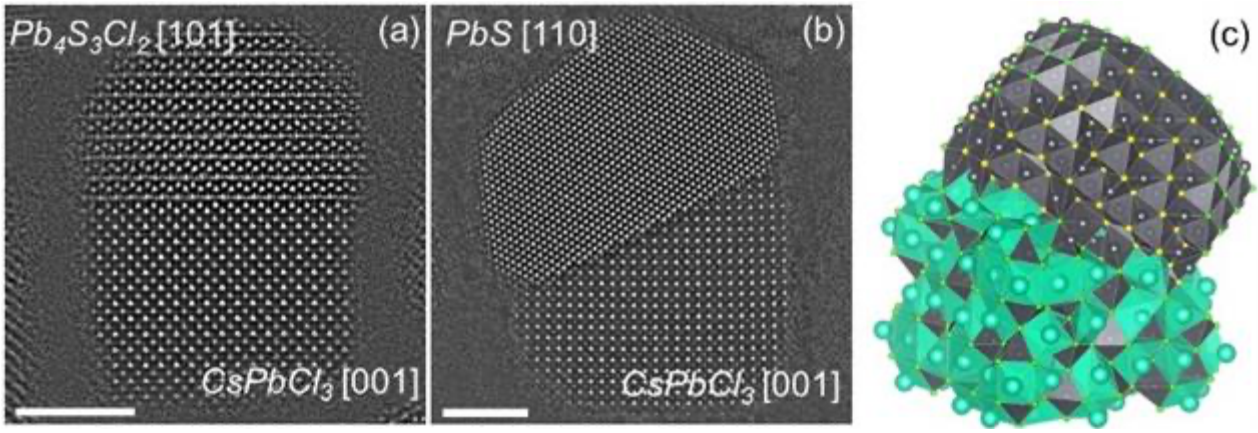

Keywords:

Quantum dots, perovskites, HRSTEM

Reference:

[1] Livakas, N. et al. J. Am. Chem. Soc. 2023, 145, 37, 20442–20450